UNIVERSITY OF BIRMINGHAM
University of Birmingham Research at Birmingham

# Platelet glycoprotein VI and C-type lectin-like receptor 2 deficiency accelerates wound healing by impairing vascular integrity in mice

Wichaiyo, Surasak; Lax-Williams, Sian; Montague, Samantha; Li, Zhi; Grygielska, Beata; Pike, Jeremy; Haining, Elizabeth; Brill, Alexander; Watson, Steve; Rayes, Julie

*DOI:*
10.3324/haematol.2018.208363

*License:*
Creative Commons: Attribution-NonCommercial (CC BY-NC)

*Document Version*
Publisher's PDF, also known as Version of record

*Citation for published version (Harvard):*
Wichaiyo, S, Lax-Williams, S, Montague, S, Li, Z, Grygielska, B, Pike, J, Haining, E, Brill, A, Watson, S & Rayes, J 2019, 'Platelet glycoprotein VI and C-type lectin-like receptor 2 deficiency accelerates wound healing by impairing vascular integrity in mice', *Haematologica*, vol. 104, no. 8, pp. 1648-1660. https://doi.org/10.3324/haematol.2018.208363

Link to publication on Research at Birmingham portal

**Publisher Rights Statement:**
Obtained from the Haematologica Journal website http://www.haematologica.org

**General rights**
Unless a licence is specified above, all rights (including copyright and moral rights) in this document are retained by the authors and/or the copyright holders. The express permission of the copyright holder must be obtained for any use of this material other than for purposes permitted by law.

• Users may freely distribute the URL that is used to identify this publication.
• Users may download and/or print one copy of the publication from the University of Birmingham research portal for the purpose of private study or non-commercial research.
• User may use extracts from the document in line with the concept of 'fair dealing' under the Copyright, Designs and Patents Act 1988 (?)
• Users may not further distribute the material nor use it for the purposes of commercial gain.

Where a licence is displayed above, please note the terms and conditions of the licence govern your use of this document.

When citing, please reference the published version.

**Take down policy**
While the University of Birmingham exercises care and attention in making items available there are rare occasions when an item has been uploaded in error or has been deemed to be commercially or otherwise sensitive.

If you believe that this is the case for this document, please contact UBIRA@lists.bham.ac.uk providing details and we will remove access to the work immediately and investigate.

Download date: 14. Jun. 2020

Published Ahead of Print on February 7, 2019, as doi:10.3324/haematol.2018.208363.
Copyright 2019 Ferrata Storti Foundation.

haematologica
Journal of The Ferrata Storti Foundation

# Platelet glycoprotein VI and C-type lectin-like receptor 2 deficiency accelerates wound healing by impairing vascular integrity in mice

by Surasak Wichaiyo, Sian Lax, Samantha J. Montague, Zhi Li, Beata Grygielska, Jeremy A. Pike, Elizabeth J. Haining, Alexander Brill, Steve P. Watson, and Julie Rayes

Haematologica 2019 [Epub ahead of print]

*Citation: Surasak Wichaiyo, Sian Lax, Samantha J. Montague, Zhi Li, Beata Grygielska, Jeremy A. Pike, Elizabeth J. Haining, Alexander Brill, Steve P. Watson, and Julie Rayes. Platelet glycoprotein VI and C-type lectin-like receptor 2 deficiency accelerates wound healing by impairing vascular integrity in mice. Haematologica. 2019; 104:xxx doi:10.3324/haematol.2018.208363*

*Publisher's Disclaimer.*
*E-publishing ahead of print is increasingly important for the rapid dissemination of science. Haematologica is, therefore, E-publishing PDF files of an early version of manuscripts that have completed a regular peer review and have been accepted for publication. E-publishing of this PDF file has been approved by the authors. After having E-published Ahead of Print, manuscripts will then undergo technical and English editing, typesetting, proof correction and be presented for the authors' final approval; the final version of the manuscript will then appear in print on a regular issue of the journal. All legal disclaimers that apply to the journal also pertain to this production process.*

**Platelet glycoprotein VI and C-type lectin-like receptor 2 deficiency accelerates wound healing by impairing vascular integrity in mice**

Surasak Wichaiyo[1,2], Sian Lax[1], Samantha J. Montague[1], Zhi Li[3], Beata Grygielska[1], Jeremy A. Pike[4], Elizabeth J. Haining[1], Alexander Brill[1,5], Steve P. Watson[1,4,6 #], and Julie Rayes[1 #]

[1]Institute of Cardiovascular Sciences, College of Medical and Dental Sciences, University of Birmingham, Birmingham, UK.

[2]Department of Pharmacology, Faculty of Pharmacy, Mahidol University, Bangkok, Thailand.

[3]Institute of Immunology and Immunotherapy, College of Medical and Dental Sciences, University of Birmingham, Birmingham, UK.

[4]Centre of Membrane Proteins and Receptors (COMPARE), Universities of Birmingham and Nottingham, The Midlands, UK.

[5]Department of Pathophysiology, Sechenov First Moscow State Medical University, Moscow, Russia.

[6]Institute of Microbiology and Infection, College of Medical and Dental Sciences, University of Birmingham, Birmingham, UK.

Running title: Platelet GPVI and CLEC-2 in skin wound healing

Correspondence: [#]Steve P. Watson, email: s.p.watson@bham.ac.uk

[#]Julie Rayes, email: j.rayes@bham.ac.uk

Word count: abstract 234 words, manuscript 3607 words, 0 table, 8 figures, 46 references, supplemental material 1 file (contains 1 table and 10 figures)

**Abstract**

Platelets promote wound healing by forming a vascular plug and by secreting growth factors and cytokines. Glycoprotein (GP)VI and C-type lectin-like receptor (CLEC)-2 signal through a (hem)-immunoreceptor tyrosine-based activation motif, which induce platelet activation. GPVI and CLEC-2 support vascular integrity during inflammation in the skin through regulation of leukocyte migration and function, and by sealing sites of vascular damage. In this study, we have investigated the role of impaired vascular integrity due to GPVI and/or CLEC-2 deficiency in wound repair using a full-thickness excisional skin wound model in mice. Transgenic mice deficient in both GPVI and CLEC-2 exhibited accelerated skin wound healing, despite a marked impairment in vascular integrity. The local and temporal bleeding in the skin led to greater plasma protein entry, including fibrinogen and clotting factors, was associated with increased fibrin generation, reduction in wound neutrophils and M1 macrophages, decreased level of tumor necrosis factor (TNF)-α, and enhanced angiogenesis at day 3 after injury. Accelerated wound healing was not due to developmental defects in CLEC-2 and GPVI double-deficient mice as similar results were observed in GPVI-deficient mice treated with a podoplanin-blocking antibody. The rate of wound healing was not altered in mice deficient in either GPVI or CLEC-2. Our results show that contrary to defects in coagulation, bleeding following a loss of vascular integrity caused by platelet CLEC-2 and GPVI deficiency facilitates wound repair by increasing fibrin(ogen) deposition, reducing inflammation, and promoting angiogenesis.

## Introduction

Cutaneous wound repair is a complex process, which requires a well-regulated interplay between diverse cell types and molecules.[1] Four interrelated phases of wound healing have been described namely hemostasis, inflammation, proliferation, and remodeling.[1] Immediately upon injury, platelets and fibrin generate a hemostatic plug to prevent excessive blood loss. Additionally, the fibrin clot forms a scaffold to promote migration of local cells surrounding the wound.[2] Deficiency in clotting factors, including tissue factor (TF), factor (F)VII or FIX, results in persistent intra-tissue bleeding and delayed wound healing.[3-5] Shortly after, neutrophils and inflammatory macrophages (M1) are recruited to eliminate microbes and cellular debris, driving the inflammatory phase.[1,6] During the proliferative phase, re-epithelialization and angiogenesis promote cell growth and wound recovery. In addition, fibroblasts infiltrate the granulation tissue to produce extracellular matrix proteins, and to differentiate into myofibroblasts, mediating wound contraction.[1] In parallel, the number of M2 reparative macrophages increases, contributing to resolution of inflammation.[1,6] Complete wound closure and re-organization of collagen fibers restore skin integrity during the remodeling phase.[1]

Platelets play several roles in wound healing during the hemostatic, inflammatory, and vascular repair phases.[7] Platelets secrete chemoattractants and growth factors that mediate cell recruitment and tissue repair, respectively.[1,7,8] This is illustrated by the delay in healing of corneal epithelial abrasion in thrombocytopenic and P-selectin-deficient mice.[9] Moreover, platelet-rich plasma, which contains growth factors, promotes skin wound healing in mice[10] and is a possible therapeutic agent to facilitate wound repair.

Platelet immunoreceptor tyrosine-based activation motif (ITAM) receptors, GPVI and CLEC-2, share a common Src/Syk/PLCγ2-dependent signaling pathway leading to platelet activation.[11] A primary role

for GPVI and a secondary role for CLEC-2 in maintaining vascular integrity in the inflamed skin has been demonstrated.[12,13] In addition, CLEC-2 and GPVI are key regulators of inflammation. GPVI promotes a pro-inflammatory phenotype during glomerulonephritis[14], arthritis[15], and dermatitis[16]. The CLEC-2-podoplanin axis is anti-inflammatory and protects against organ damage during lung and systemic inflammation.[17,18]

Due to the complex interplay between platelets and inflammation during wound healing, we hypothesize that GPVI and/or CLEC-2 regulate vascular integrity during wound repair and alter the healing process. In the present study, we show that deletion of both CLEC-2 and GPVI accelerates wound healing in a mouse model of full-thickness excisional skin wound repair. This is associated with a transient and self-limited bleeding (i.e. due to impaired vascular integrity), fibrin(ogen) matrix deposition, a reduction in wound neutrophils and M1 macrophages, and increased angiogenesis during the inflammatory phase. Taken together, we show that impaired vascular integrity-induced bleeding is beneficial during a model of sterile wound healing.

## Methods

### *Animals*

Male and female WT, platelet-specific CLEC-2-deficient (*Clec1b*$^{fl/fl}$*Pf4-Cre*), GPVI knockout (*Gp6*$^{-/-}$), and CLEC-2/GPVI double-deficient (*Clec1b*$^{fl/fl}$*Pf4-Cre/Gp6*$^{-/-}$; DKO) mice aged 8-10 weeks were used. All experiments were performed in accordance with UK laws (Animal [Scientific Procedures] Act 1986) with approval of local ethics committee and UK Home Office under PPL P0E98D513 and P14D42F37, respectively.

*Full-thickness excisional skin wound model*

A single full-thickness excisional skin wound was made on the shaved flank skin of mice using a 4 mm-diameter biopsy punch (Kai Industries, Japan). Wounds were imaged using a Nikon COOLPIX B500 digital camera each day and wound size measured using calipers[19] on a daily basis for up to nine days post-injury. Wound area was calculated as described[19] and presented as the percentage of initial wound size[10]. In a second set of experiments, anti-podoplanin antibody (clone 8.1.1, 100 µg)[13,17,20] or IgG isotype control were intravenously injected 24 hours before and again 24 hours after wounding. Wound size was monitored for three days post-injury.

*Other associated methods*

For details, see supplemental materials.

**Results**

*CLEC-2 and GPVI ligands are present within perivascular areas during skin wounding*

In unchallenged WT mouse skin, collagen was abundantly expressed throughout the dermis and hypodermis, including around blood vessels, and podoplanin was predominantly expressed on lymphatic endothelial cells and on perivascular cells (Figure S1A, B). At day 3 post-wounding, podoplanin expression was also observed surrounding blood vessels in WT and transgenic mice (Figure 1A). These podoplanin-expressing cells included pericytes (neuron-glial antigen 2; $NG2^+$) (Figure 1A), fibroblasts ($vimentin^+$), infiltrating monocytes ($Ly6C^+$) and macrophages ($F4/80^+$) (Figure 1B). In addition, podoplanin was upregulated on migrating keratinocytes, and on stromal and infiltrating cells within the granulation tissue (Figure S1C). The level of perivascular podoplanin was increased in

*Clec1b*$^{fl/fl}$*Pf4-cre* mice compared to WT mice (Figure 1A, B). In DKO mice, podoplanin expression was similar to that observed in WT and *Gp6*$^{-/-}$ mice (Figure 1A, B).

Three days after wound injury, platelets (CD41$^{+}$) were observed in close proximity to the vessel wall (surrounded by pericytes) in WT, *Clec1b*$^{fl/fl}$*Pf4-cre, and Gp6*$^{-/-}$ mice (Figure 1A arrow). In DKO mice, platelets were more widely distributed, including at the vessel wall and in the surrounding tissue (Figure 1A star). The platelet count in *Clec1b*$^{fl/fl}$*Pf4-cre* and DKO mice was approximately 25% and 40% lower than in WT, respectively (Figure S1D) and was not altered by wound injury.

These results demonstrate that platelets are present in perivascular areas during the initial wound healing process in mouse skin where the ligands for GPVI and CLEC-2 are also observed. Deletion of CLEC-2 from platelets is associated with increased podoplanin-expressing cells in the perivascular space during wound healing while concurrent ablation with GPVI reverses this phenotype.

*Cutaneous wound healing is accelerated in mice deficient in platelet CLEC-2 and GPVI*

To determine the contribution of platelet ITAM receptors in wound repair, we monitored the time course of wound closure in WT and platelet ITAM receptor(s)-deficient mice. All mouse strains exhibited complete wound closure within nine days post-injury (Figure 2A). However, mice deficient in both GPVI and CLEC-2 demonstrated accelerated repair (Figure 2B), characterized by the presence of a dark scab and redness around the wound (Figure 2A), especially within the first three days after injury compared to WT and single ITAM-deficient mice. There was no discernable difference in wound appearance in all mouse strains after four days post-injury (Figure 2A) and wound size was not macroscopically different at day 9 post-injury (Figure 2B). However, the morphometric analysis of skin histology at this time revealed a significant smaller scar in DKO mice, as shown by a shorter length of

hyperplastic epidermis compared to WT and *Clec1b*$^{fl/fl}$*Pf4-cre* mice (Figure 2C, D) and a narrower inter-subcutaneous gap than WT mice (Figure 2C, E).

At day 3 post-injury, re-epithelialization was observed in all groups (Figure 3A). However, this process was enhanced in DKO mice compared to WT and *Clec1b*$^{fl/fl}$*Pf4-cre* mice but not *Gp6*$^{-/-}$ mice (Figure 3B). There was no significant difference in wound contraction between all tested groups (Figure 3C). DKO mice also had a larger area of granulation tissue compared to WT mice (Figure 3A, D). Improved wound healing was associated with enhanced angiogenesis as assessed by the increase in CD31$^{+}$ area in DKO animals at day 3 post-injury (Figure 3E, F) although the density of blood vessels (CD31$^{+}$) and lymphatic vessels (podoplanin$^{+}$) in unchallenged skin was similar among all groups (Figure S1E, F).

These results demonstrate that deletion of both CLEC-2 and GPVI accelerates skin wound closure, enhances re-epithelialization and angiogenesis, and reduces scar formation.

*GPVI and CLEC-2 maintain vascular integrity during the inflammatory phase of wound repair*

The redness surrounding the wound in DKO mice in the inflammatory phase is indicative of increased vascular leakiness. Macroscopic examination of the skin at day 3 post-injury demonstrated vasodilation and bleeding into the wound as well as into the surrounding skin in DKO mice, with less severe vascular leakage seen in *Gp6*$^{-/-}$ mice (Figure 4A). H&E staining confirmed the extravasation of red blood cells (RBCs) in the dermis at the edge of the wound at day 3 post-injury in both DKO and *Gp6*$^{-/-}$ mice (Figure S2A). Clearance of extravascular RBCs was observed at day 9 post-injury in all groups (Figure S2B). Due to blood/lymphatic mixing phenotype in DKO and to a lesser degree in *Clec1b*$^{fl/fl}$*Pf4-cre* mice, RBCs were also present in lymphatic vessels (podoplanin$^{+}$) (Figure S2C).

These observations demonstrate marked impairment of vascular integrity during the inflammatory phase of wound repair in DKO mice with a milder phenotype in *Gp6*$^{-/-}$ mice. Vascular leakage is diminished in later phases when inflammation subsides.

*GPVI and CLEC-2 deficiency increases fibrin(ogen) deposition during the inflammatory phase of repair*

Increased vascular permeability results in leakage of blood cells and plasma proteins into the wound[21] where they come in contact with TF[5,22], which activates the extrinsic pathway of blood coagulation. An increase in fibrinogen deposition was particularly marked in the granulation tissue at day 3 post-injury (Figure 4B, C) with no significant alteration in TF expression in DKO mice (Figure S3A, B). Fibrin content in the wound scab was similar between WT and DKO mice at day 1 post-injury (Figure S3C, D), but was significantly increased in the DKO mice at day 3 post-injury, compared to WT and *Clec1b*$^{fl/fl}$*Pf4-cre* mice but not to *Gp6*$^{-/-}$ mice, which exhibited a more moderate vascular leakage (Figure 4D, E). At day 9 post-injury, fibrin was mainly located on the upper part of the scar in all groups (Figure 4F) and was notably lower in the DKO mice compared to WT and *Gp6*$^{-/-}$ mice (Figure 4G). There was no significant difference in wound (myo)fibroblasts (Figure S3E-G) and collagen content (Figure S3H, I) between DKO mice and WT at day 3 and day 9 post-injury.

These results indicate that the loss of vascular integrity during the inflammatory phase increases extravasation of plasma proteins, including fibrinogen and clotting factors, into the wound of DKO mice. The increase in fibrinogen and fibrin deposition is associated with accelerated wound healing and is then cleared from the healing wound.

*Platelet ITAM receptor deficiency reduces wound neutrophils and M1 macrophages during the inflammatory phase*

The influx of inflammatory cells was investigated at days 1, 3, and 9 post-injury. Neutrophil ($Gr\text{-}1^+$) infiltration on day 1 post-injury was similar between WT and DKO mice (Figure S4A, B). At day 3 post-injury, DKO mice showed a significant impairment in neutrophil infiltration compared to WT and *Clec1b*$^{fl/fl}$*Pf4-cre* mice but not *Gp6*$^{-/-}$ mice (Figure 5A, B). The decrease in neutrophil infiltration was confirmed using anti-Ly6G antibody clone 1A8 (data not shown). A two-fold increase in wound neutrophils was observed in WT but not in DKO mice at this time relative to day 1 post-injury (Figure 5C). At day 9 post-injury, DKO mice showed higher number in wound neutrophils than WT (Figure 5D, E) although neutrophil level was significantly decreased in both groups relative to day 1 and day 3 post-injury (Figure 5C). Blood neutrophil counts were similar in unchallenged mice across all groups (Figure 5F). At day 3 post-injury, the number of blood neutrophils was significantly decreased in WT and *Clec1b*$^{fl/fl}$*Pf4-cre* (Figure 5F) while remaining unaltered during the time course of wound healing in DKO and *Gp6*$^{-/-}$ mice (Figure 5F). The decrease in neutrophil infiltration was not due to a defect of chemoattractants at the wound site as measured by the presence of chemokine CXCL-1 (Figure S6A, B) or platelet factor 4 (PF4) (Figure S6C, D). *In vitro* migration towards N-formyl-methionyl-leucyl-phenylalanine (fMLP) using bone marrow-derived neutrophils demonstrated that migration of neutrophils from WT mice was attenuated by fibrinogen, and strongly inhibited by crosslinked fibrin compared to the migration through collagen (Figure S7). Fibrinogen and fibrin showed a similar degree of inhibition for the migration of neutrophils from DKO mice (Figure S7).

There was no significant difference in wound monocytes ($Ly6C^+$) at day 1 post-injury between DKO mice and WT (Figure S4C, D). At day 3 post-injury, DKO mice showed a significantly higher number of

wound monocytes compared to all other strains (Figure 6A, B), which was reflected by a four-fold increase in wound monocytes relative to day 1 post-injury (Figure 6C). At day 9 post-injury, monocytes within the wound remained at low level in WT and single-knockout mice (Figure 6D, E). Wound monocytes in DKO mice were decreased at this time relative to day 3 post-injury (Figure 6C), but remained higher than other groups (Figure 6D, E). In blood, *Clec1b*$^{fl/fl}$*Pf4-cre* exhibited an increase in baseline circulating monocytes compared to WT and DKO mice (Figure S4G, left). Blood monocytes were greatly reduced at day 3 and day 9 post-injury in all groups compared to their unchallenged controls (Figure 6F). However, the level of blood monocytes in DKO mice was significantly higher than *Clec1b*$^{fl/fl}$*Pf4-cre* mice at day 3 post-injury (Figure S4G, middle) and then all groups at day 9 post-injury (Figure S4G, right).

The influx of macrophages (F4/80$^{+}$) in DKO mice was reduced at day 1 post-injury compared to WT (Figure S4E, F). At day 3 post-injury, wound macrophages in *Clec1b*$^{fl/fl}$*Pf4-cre* mice were elevated, compared to all other strains (Figure 7A, B). A six-fold increase in wound macrophages was observed in WT mice at day 3 relative to day 1 post-injury (Figure 7C). DKO mice showed a significant reduction in macrophages compared to WT but not *Gp6*$^{-/-}$ mice at this time (Figure 7B, C). Inducible nitric oxide synthase (iNOS)-expressing macrophages (M1 phenotype) (Figure 7D, E) and TNF-α level (Figure 7G, H) within the wound of DKO mice were decreased whereas Fizz-1-positive macrophages (a M2 marker) were similar to WT (Figure S5D, E) at day 3 post-injury. At day 9 post-injury, wound macrophages in DKO mice were similar to WT and *Clec1b*$^{fl/fl}$*Pf4-cre* mice (Figure S5D, E) with no difference in M1 (Figure 7D, F) and M2 macrophages (Figure S5A, C) between WT and DKO strains. *Gp6*$^{-/-}$ mice showed a lower number of macrophages within the wound scar than in *Clec1b*$^{fl/fl}$*Pf4-cre* mice at day 9 post-injury (Figure S5E).

Overall, these data illustrate that CLEC-2 deletion promotes leukocyte sequestration in the wound during the inflammatory phase, especially macrophages. Deletion of both ITAM receptors leads to a significant reduction in wound neutrophils and M1 macrophages during this phase and a decrease in TNF-α expression in the tissue.

*Inhibition of CLEC-2-podoplanin axis accelerates wound healing in GPVI-deficient mice*

*Clec1b*$^{fl/fl}$*Pf4-cre* and DKO mice present with blood/lymphatic mixing and moderate thrombocytopenia.[11,17] To investigate the influence of these defects on wound healing, we injected *Gp6*$^{-/-}$ mice with an antibody to podoplanin (anti-podoplanin-treated *Gp6*$^{-/-}$ mice) that blocks CLEC-2-podoplanin interaction. A significant acceleration in wound healing was observed in anti-podoplanin-treated *Gp6*$^{-/-}$ mice at day 2 and day 3 post-injury (Figure 8A, B), in association with enhanced vascular leakage (Figure 8A, C) and increased fibrin deposition (Figure 8D, E). Moreover, decreased wound neutrophils (Figure 8F, G) and macrophages (Figure 8H, I), and higher wound monocytes (Figure S8A, B) but unaltered level of TNF-α (Figure S8C, D) were observed in anti-podoplanin-treated *Gp6*$^{-/-}$ mice. The re-epithelialization (Figure S8E, F), granulation tissue formation (Figure S8E, H) and angiogenesis (Figure S8I, J) were also increased in anti-podoplanin-treated *Gp6*$^{-/-}$ mice. However, wound contraction was not significantly changed (Figure S8E, G). Similar to DKO mice, extravasation of platelets was detected together with the presence of anti-podoplanin antibody on pericytes and other perivascular cells in anti-podoplanin-treated *Gp6*$^{-/-}$ mice at this time (Figure S9).

These data indicate that the accelerated wound healing in DKO mice is not due to developmental defects or thrombocytopenia, but due to a combined loss of the interaction of platelet CLEC-2 and GPVI with their respective ligands.

**Discussion**

In this study, we show that combined deletion of platelet CLEC-2 and GPVI promotes healing of a full-thickness skin wound in mice compared to WT or single-knockout mice. The accelerated wound closure is accompanied by impairment of vascular integrity, rapid re-epithelialization and an increase in granulation tissue formation, resulting in a smaller wound scar. This is also associated with elevated levels of fibrinogen and fibrin in the tissue, reduced infiltration of leukocytes, and enhanced angiogenesis. A proposed model for the multifactorial regulation of accelerated wound healing in the absence of the two ITAM receptors is shown in Figure S10.

Wound healing is a multistep process involving coagulation, vascular permeability changes, inflammation, cell proliferation and cell migration.[1,2,21] In our study, we show that deletion of CLEC-2 and GPVI in platelets leads to increased bleeding into the wound, in association with accelerated wound repair. These effects are not due to blood/lymphatic vessel mixing or the reduction in platelet count in the DKO mice as similar results were observed in anti-podoplanin-antibody treated *Gp6*$^{-/-}$ mice, which do not have these defects. Acceleration of wound healing is also observed in mice treated with histamine[23] or serum fraction of the natural latex from rubber tree[21], which enhances vascular permeability, a milder form of vascular leakage. Therefore, impaired vascular integrity as seen in the DKO platelets or increased permeability leads to extravasation of growth factors, cytokines, and plasma proteins to the tissue, and promotion of wound healing.

The role of blood coagulation in wound repair has been studied in mice expressing low TF[5] or lacking FIX (hemophilia B mice)[3,5]. In these two models, the deficiency in clotting factors leads to a persistent hematoma formation (due to a prolonged subcutaneous bleeding) and a reduction in fibrin generation,

both of which contribute to a delay in wound repair. Chronic hemorrhage also contributes to the non-healing wound characteristics in cancers, which promotes tumor growth.[24-26] In contrast, we show that in the presence of an intact coagulation cascade, the transient and self-limited bleeding into the wound (which is rich in TF[5,22]) caused by the impairment of vascular integrity at an initial stage, is associated with accelerated wound repair. This is most likely due to increased entry of platelets, clotting factors, and plasma proteins, leading to fibrinogen accumulation and fibrin generation. Thus, the mechanism of bleeding determines whether it is beneficial or detrimental in wound repair.

Fibrinogen and fibrin are not only crucial for clot formation, but also act as a natural suture/sealant, providing a matrix for cell migration as well as a reservoir for growth factors and cytokines.[2] For example, fibrin exposes plasminogen to migrating keratinocytes, which in turn convert plasminogen into plasmin to mediate fibrinolysis, allowing the cells to move along the fibrin(ogen) matrix.[27-29] Similarly, endothelial cells proliferate and migrate over fibrin(ogen), form a capillary tube, contributing to angiogenesis during wound healing.[30-32] In DKO mice, we therefore propose that fibrin(ogen) accumulation promotes re-epithelialization and angiogenesis and accelerate wound repair.

In contrast, fibrinogen[33] and a high concentration of fibrin[34] inhibit neutrophil migration as previously reported and in line with our *in vitro* data. These data may explain our observations that in DKO mice, wound neutrophils at day 3 did not increase over the amount seen at day 1 post-injury. This is in contrast to wound neutrophil accumulation in WT, which was higher at day 3 than at day 1 post-injury. Increased fibrin content in the wound was also observed in DKO mice compared to WT at day 3 post injury. Therefore, the physical obstruction and anti-migratory properties of the fibrin clot is likely to inhibit neutrophil wound entry observed in DKO mice. Moreover, given that the level of blood neutrophils at this early phase was not significantly different between WT and DKO mice, altered

neutrophil turnover/apoptosis in DKO mice is unlikely to significantly contribute to the reduction in wound neutrophils observed in DKO compared to WT at day 3 post-injury.

Consistent with our data, several lines of evidence demonstrate improved wound healing in neutrophil-depleted conditions.[35-38] Indeed, neutrophil infiltration mediates damage through a production of proteases[35], oxidative radicals, elastase[39], and neutrophil extracellular traps[37], all of which can delay the healing process. A similar effect of fibrin(ogen) might also apply to monocyte/macrophage recruitment since fibrinogen has an anti-adhesive effect against monocytes.[40] A recent sterile wound model has demonstrated that $Ly6C^+$ monocytes are present throughout wound healing and differentiate into M1 macrophages during inflammatory phase and M2 macrophages during the reparative phase.[41] In addition, it has been shown that TNF-α secretion is increased during monocyte-to-M1-macrophage differentiation.[41,42] The reduction in TNF-α during the inflammatory phase is associated with the increase in wound monocytes but not macrophages suggests an inhibition in monocyte-to-M1-macrophage transition in DKO mice, resulting in a significant change in immune cell infiltration in the wound.

Depletion of macrophages in the first five days has previously been shown to delay the later stages of wound closure, but not during the inflammatory phase (day 1-3).[43] This is due to a decrease in M2 macrophages[43], supporting our observation that a reduction in wound macrophages, particularly M1 phenotype, in the early phase does not negatively affect wound closure but may contribute to the reduction in scar formation[43]. The alteration in M2 macrophages was not observed in DKO mice although the previous dermatitis model has reported an increase number of M2 phenotypes in GPVI-deficient mice[16], suggesting other contributing factors for macrophage polarization during skin wound healing[6].

The increased risk of wound contamination is a concern in the context of intra-tissue bleeding and reduced wound leukocytes. However, it has recently been shown that rapid formation of a fibrin film over the surface of the wound is protective against bacterial infection.[44] This process might also reduce the need for leukocyte infiltration to kill microbes. Moreover, a previous study has reported that a two-fold increase in wound neutrophils is driven by *Staphylococcus aureus* infection.[45] Whether the beneficial potential of targeting GPVI and CLEC-2 might modulate the risk of wound infection requires further investigation.

In conclusion, we show that deletion of platelet GPVI and CLEC-2 facilitates cutaneous wound repair through a local and temporal vascular leakage leading to increased fibrin(ogen) deposition and reduced leukocyte infiltration. Thus, impaired vascular integrity due to the loss of GPVI and CLEC-2 is beneficial to wound repair. This contrasts with results in coagulation-deficient mice, with differences explained by altered formation of fibrin and most likely alteration in immune cell trafficking. A shorter duration of healing lowers the risk of complications (e.g. infection) and the cost of wound care.[46] Based on our study, targeting CLEC-2 and GPVI at the wound site together with optimal wound care (e.g. aseptic dressing) might represent a new pathway to promote healing and reduce scar formation.

**Acknowledgements**

This work was supported by the Ministry of Sciences and Technology of Thailand and the British Heart Foundation (RG/13/18/30563). S.P.W. holds a BHF Chair (CH03/003). The authors would like to thank the BMSU at the University of Birmingham for technical support in animal experiments and the Technology Hub for imaging assistance.

**Conflict-of-interest disclosure**

The authors declare no competing financial interests

**Authorship**

Contribution: S.W., S.P.W., J.R., S.L., A.B. designed the study. S.W., J.R., S.L. performed experiments. S.J.M., Z.L., B.G., E.J.H. helped with the setup of experiments. S.W., J.R., S.L., S.P.W., A.B. analyzed the data. J.A.P., E.J.H. contributed to data analysis. S.W., J.R., S.P.W. wrote the manuscript. All authors reviewed and approved this manuscript.

**Footnotes**

S.J.M currently works at ACRF Department of Cancer Biology and Therapeutics, The Australian National University, Canberra, 2601, ACT, Australia.

**References**


1. Shaw TJ, Martin P. Wound repair at a glance. J Cell Sci. 2009;122(Pt 18):3209-3213.
2. Drew AF, Liu H, Davidson JM, Daugherty CC, Degen JL. Wound-healing defects in mice lacking fibrinogen. Blood. 2001;97(12):3691-3698.
3. Hoffman M, Harger A, Lenkowski A, Hedner U, Roberts HR, Monroe DM. Cutaneous wound healing is impaired in hemophilia B. Blood. 2006;108(9):3053-3060.
4. Xu Z, Xu H, Ploplis VA, Castellino FJ. Factor VII deficiency impairs cutaneous wound healing in mice. Mol Med. 2010;16(5-6):167-176.
5. Monroe DM, Mackman N, Hoffman M. Wound healing in hemophilia B mice and low tissue factor mice. Thromb Res. 2010;125 Suppl 1:S74-77.
6. Sindrilaru A, Scharffetter-Kochanek K. Disclosure of the Culprits: Macrophages-Versatile Regulators of Wound Healing. Adv Wound Care (New Rochelle). 2013;2(7):357-368.
7. Golebiewska EM, Poole AW. Platelet secretion: From haemostasis to wound healing and beyond. Blood Rev. 2015;29(3):153-162.
8. Brill A, Elinav H, Varon D. Differential role of platelet granular mediators in angiogenesis. Cardiovasc Res. 2004;63(2):226-235.
9. Li Z, Rumbaut RE, Burns AR, Smith CW. Platelet response to corneal abrasion is necessary for acute inflammation and efficient re-epithelialization. Invest Ophthalmol Vis Sci. 2006;47(11):4794-4802.
10. Yang HS, Shin J, Bhang SH, et al. Enhanced skin wound healing by a sustained release of growth factors contained in platelet-rich plasma. Exp Mol Med. 2011;43(11):622-629.
11. Bender M, May F, Lorenz V, et al. Combined in vivo depletion of glycoprotein VI and C-type lectin-like receptor 2 severely compromises hemostasis and abrogates arterial thrombosis in mice. Arterioscler Thromb Vasc Biol. 2013;33(5):926-934.
12. Gros A, Syvannarath V, Lamrani L, et al. Single platelets seal neutrophil-induced vascular breaches via GPVI during immune-complex-mediated inflammation in mice. Blood. 2015;126(8):1017-1026.
13. Rayes J, Jadoui S, Lax S, et al. The contribution of platelet glycoprotein receptors to inflammatory bleeding prevention is stimulus and organ dependent. Haematologica. 2018;103(6):e256-e258.

14. Devi S, Kuligowski MP, Kwan RY, et al. Platelet recruitment to the inflamed glomerulus occurs via an alphaIIbbeta3/GPVI-dependent pathway. Am J Pathol. 2010;177(3):1131-1142.
15. Boilard E, Nigrovic PA, Larabee K, et al. Platelets amplify inflammation in arthritis via collagen-dependent microparticle production. Science. 2010;327(5965):580-583.
16. Pierre S, Linke B, Suo J, et al. GPVI and Thromboxane Receptor on Platelets Promote Proinflammatory Macrophage Phenotypes during Cutaneous Inflammation. J Invest Dermatol. 2017;137(3):686-695.
17. Rayes J, Lax S, Wichaiyo S, et al. The podoplanin-CLEC-2 axis inhibits inflammation in sepsis. Nat Commun. 2017;8(1):2239.
18. Lax S, Rayes J, Wichaiyo S, et al. Platelet CLEC-2 protects against lung injury via effects of its ligand podoplanin on inflammatory alveolar macrophages in the mouse. Am J Physiol Lung Cell Mol Physiol. 2017;313(6):L1016-L1029.
19. Moreira CF, Cassini-Vieira P, da Silva MF, Barcelos LS. Skin Wound Healing Model - Excisional Wounding and Assessment of Lesion Area. Bio-protocol. 2015;5(22):e1661.
20. Payne H, Ponomaryov T, Watson SP, Brill A. Mice with a deficiency in CLEC-2 are protected against deep vein thrombosis. Blood. 2017;129(14):2013-2020.
21. Mendonca RJ, Mauricio VB, Teixeira Lde B, Lachat JJ, Coutinho-Netto J. Increased vascular permeability, angiogenesis and wound healing induced by the serum of natural latex of the rubber tree Hevea brasiliensis. Phytother Res. 2010;24(5):764-768.
22. Chen J, Kasper M, Heck T, et al. Tissue factor as a link between wounding and tissue repair. Diabetes. 2005;54(7):2143-2154.
23. Numata Y, Terui T, Okuyama R, et al. The accelerating effect of histamine on the cutaneous wound-healing process through the action of basic fibroblast growth factor. J Invest Dermatol. 2006;126(6):1403-1409.
24. McDonald DM, Baluk P. Significance of blood vessel leakiness in cancer. Cancer Res. 2002;62(18):5381-5385.
25. Dvorak HF. Tumors: wounds that do not heal-redux. Cancer Immunol Res. 2015;3(1):1-11.
26. Yin T, He S, Liu X, et al. Extravascular red blood cells and hemoglobin promote tumor growth and therapeutic resistance as endogenous danger signals. J Immunol. 2015;194(1):429-437.

27. Kubo M, Van de Water L, Plantefaber LC, et al. Fibrinogen and fibrin are anti-adhesive for keratinocytes: a mechanism for fibrin eschar slough during wound repair. J Invest Dermatol. 2001;117(6):1369-1381.
28. Ronfard V, Barrandon Y. Migration of keratinocytes through tunnels of digested fibrin. Proc Natl Acad Sci U S A. 2001;98(8):4504-4509.
29. Geer DJ, Andreadis ST. A novel role of fibrin in epidermal healing: plasminogen-mediated migration and selective detachment of differentiated keratinocytes. J Invest Dermatol. 2003;121(5):1210-1216.
30. Chalupowicz DG, Chowdhury ZA, Bach TL, Barsigian C, Martinez J. Fibrin II induces endothelial cell capillary tube formation. J Cell Biol. 1995;130(1):207-215.
31. Laurens N, Koolwijk P, de Maat MP. Fibrin structure and wound healing. J Thromb Haemost. 2006;4(5):932-939.
32. Sahni A, Francis CW. Vascular endothelial growth factor binds to fibrinogen and fibrin and stimulates endothelial cell proliferation. Blood. 2000;96(12):3772-3778.
33. Higazi AA, Barghouti, II, Ayesh SK, Mayer M, Matzner Y. Inhibition of neutrophil activation by fibrinogen. Inflammation. 1994;18(5):525-535.
34. Hanson AJ, Quinn MT. Effect of fibrin sealant composition on human neutrophil chemotaxis. J Biomed Mater Res. 2002;61(3):474-481.
35. Dovi JV, He LK, DiPietro LA. Accelerated wound closure in neutrophil-depleted mice. J Leukoc Biol. 2003;73(4):448-455.
36. Mori R, Kondo T, Ohshima T, Ishida Y, Mukaida N. Accelerated wound healing in tumor necrosis factor receptor p55-deficient mice with reduced leukocyte infiltration. FASEB J. 2002;16(9):963-974.
37. Wong SL, Demers M, Martinod K, et al. Diabetes primes neutrophils to undergo NETosis, which impairs wound healing. Nat Med. 2015;21(7):815-819.
38. Stavrou EX, Fang C, Bane KL, et al. Factor XII and uPAR upregulate neutrophil functions to influence wound healing. J Clin Invest. 2018;128(3):944-959.
39. Wilgus TA, Roy S, McDaniel JC. Neutrophils and Wound Repair: Positive Actions and Negative Reactions. Adv Wound Care (New Rochelle). 2013;2(7):379-388.

40. Lishko VK, Burke T, Ugarova T. Antiadhesive effect of fibrinogen: a safeguard for thrombus stability. Blood. 2007;109(4):1541-1549.
41. Crane MJ, Daley JM, van Houtte O, Brancato SK, Henry WL, Jr., Albina JE. The monocyte to macrophage transition in the murine sterile wound. PLoS One. 2014;9(1):e86660.
42. Francke A, Herold J, Weinert S, Strasser RH, Braun-Dullaeus RC. Generation of mature murine monocytes from heterogeneous bone marrow and description of their properties. J Histochem Cytochem. 2011;59(9):813-825.
43. Lucas T, Waisman A, Ranjan R, et al. Differential roles of macrophages in diverse phases of skin repair. J Immunol. 2010;184(7):3964-3977.
44. Macrae FL, Duval C, Papareddy P, et al. A fibrin biofilm covers blood clots and protects from microbial invasion. J Clin Invest. 2018;128(8):3356-3368.
45. Kim MH, Liu W, Borjesson DL, et al. Dynamics of neutrophil infiltration during cutaneous wound healing and infection using fluorescence imaging. J Invest Dermatol. 2008;128(7):1812-1820.
46. Lindholm C, Searle R. Wound management for the 21st century: combining effectiveness and efficiency. Int Wound J. 2016;13 Suppl 2:5-15.

**Figure legends:**

**Figure 1. Podoplanin-expressing cells are present at perivascular area in contact with platelets during skin wound repair.** (A) Immunofluorescence staining of NG2 (red), podoplanin (green) and CD41 (white) illustrates platelets and podoplanin-expressing pericytes ($NG2^+$) around blood vessel at day 3 after injury (n=5-7). Hoechst counterstains nuclei (blue). BV = blood vessel. Arrow points to platelets at perivascular site. Star indicates extravascular localization of platelets. Scale bar = 20 µm. (B) Podoplanin (green) was double-stained with either vimentin (red; *top panel*) or Ly6C (red; *middle panel*) or F4/80 (red; *bottom panel*), which are located around blood vessel (surrounded by $NG2^+$ pericytes) at day 3 after injury (n=4-5). Scale bar = 20 µm.

**Figure 2. Deletion of platelet ITAM receptors accelerates skin wound repair process.** Mice were subjected to a full-thickness excisional skin wound and wound closure monitored for 9 days after injury. (A) Macroscopic appearance of wound at indicated time points. (B) Changes of wound size over 9 days post-injury (n=10-13). (C) H&E staining at day 9 post-injury (n=9-13). a = length of hyperplastic epidermis, b = inter-subcutaneous distance. Scale bar = 200 µm. (D) Measurement of the length of hyperplastic epidermis. (E) Measurement of inter-subcutaneous distance. All graphs are presented as mean ± SEM. Kinetics of wound closure (B) are analyzed by two-way ANOVA with Bonferroni's multiple comparison test. **p<0.05*, ***p<0.01*. *WT vs. DKO, $^{+}$*Clec1b*$^{fl/fl}$*Pf4-cre* vs DKO, $^{\#}$*Gp6*$^{-/-}$ vs. DKO. Other parameters are analyzed by one-way ANOVA with Bonferroni's multiple comparison test. **p<0.05.*

**Figure 3. Enhanced re-epithelialization and angiogenesis occur at the early phase of wound healing in the absence of GPVI and CLEC-2.** (A) H&E staining at day 3 post-injury (n=6-9). Dotted line indicates hyperplastic coverages. Black arrow points to wound edge. Red arrow indicates gap between epithelial tongues. S = scab, G = granulation tissue. Scale bar = 500 µm. (B) Measurement of re-epithelialization. (C) Measurement of wound contraction. (D) Quantification of granulation tissue area. (E) Detection of endothelial cells ($CD31^+$ cells; green) in wound area at day 3 post-injury. Hoechst counterstains nuclei (blue). Scale bar = 50 µm. (F) Quantification of $CD31^+$ area within the wound at day 3 post-injury (n=5-6). Graphs are presented as mean ± SEM and analyzed by one-way ANOVA with Bonferroni's multiple comparison test. *$p<0.05$*.

**Figure 4. Lack of platelet ITAM receptors causes local and temporal bleeding leading to fibrin(ogen) deposition during inflammatory phase of wound repair.** (A) Macroscopic images of inner side of skin wound at day 3 post-injury (n=4-6). Dotted circle indicates wound area. Arrow points to dilated vessel. Arrowhead shows bleeding into surrounding skin. (B) Fibrinogen staining (brown) of skin wound at day 3 post-injury. (C) Quantification of fibrinogen content at day 3 post-injury (n=6). (D) Martius scarlet blue (MSB) staining of skin wound at day 3 post-injury. Red = old fibrin, blue = collagen, yellow = red blood cells/fresh fibrin. (E) Quantification of fibrin content in the wound at day 3 post-injury (n=6-9). (F) MSB staining of wound scar at day 9 post-injury. (G) Quantification of fibrin content in the scar at day 9 post-injury (n=9-13). Graphs are presented as mean ± SEM and analyzed by one-way ANOVA with Bonferroni's multiple comparison test. *$p<0.05$, **$p<0.01$*. Scale bar = 200 µm.

**Figure 5. Neutrophil influx is decreased during the inflammatory phase of wound healing following platelet CLEC-2 and GPVI double-deletion.** (A) Detection of neutrophils (Gr-1 staining; brown) in wound at day 3 post-injury. (B) Quantification of neutrophils (Gr-1$^+$ cells) in wound at day 3 post-injury. *$p<0.05$, **$p<0.01$. (C) Comparison of Gr1$^+$ cells between day 1, day 3, and day 9 post-injury in WT and DKO mice. The symbols * and § indicate $p<0.05$ in WT and DKO mice, compared to the data at day 1 post-injury, respectively. The bracket shows $p<0.05$ for the comparison between day 3 and day 9 post-injury in *WT and §DKO mice, respectively. (D) Detection of neutrophils (Gr-1 staining; brown) in wound at day 9 post-injury. (E) Quantification of neutrophils (Gr-1$^+$ cells) in wound at day 9 post-injury. *$p<0.05$. (F) Comparison of blood neutrophil counts between baseline, day 3, and day 9 post-injury in each mouse strain. The symbols * and + indicate $p<0.05$ in WT and *Clec1b$^{fl/fl}$Pf4-cre* mice, compared to their control, respectively. Sample numbers in unchallenged control = 10, day 1 = 5, day 3 = 6-9, and day 9 post-injury = 9-13, respectively. Graphs are presented as mean ± SEM and analyzed by one-way ANOVA with Bonferroni's multiple comparison test. Scale bar = 20 µm.

**Figure 6. A higher number of wound monocytes is observed during the inflammatory phase of repair in mice that lack both GPVI and CLEC-2.** (A) Detection of monocytes (Ly6C$^+$ cells; brown) in wound at day 3 post-injury. (B) Quantification of Ly6C$^+$ cells in wound at day 3 post-injury (n=5-7). **$p<0.01$. (C) Comparison of Ly6C$^+$ cells between day 1, day 3, and day 9 post-injury in WT and DKO mice. The symbols * and § indicate $p<0.05$ in WT and DKO mice, compared to the data at day 1 post-injury, respectively. The bracket shows $p<0.05$ for the comparison between day 3 and day 9 post-injury in §DKO mice. (D) Detection of Ly6C$^+$ cells (brown) in wound at day 9 post-injury. (E) Quantification of Ly6C$^+$ cells in wound at day 9 post-injury (n=6). *$p<0.05$, **$p<0.01$. (F) Comparison of blood monocyte

counts between baseline, day 3, and day 9 post-injury in each mouse strain. The symbols *, +, #, and § indicate *p<0.05* in WT, *Clec1b*$^{fl/fl}$*Pf4-cre*, *Gp6*$^{-/-}$, and DKO mice, compared to their control, respectively. Sample numbers in unchallenged control = 10, day 1 = 5, day 3 = 6-9, and day 9 post-injury = 10-13, respectively. Graphs are presented as mean ± SEM and analyzed by one-way ANOVA with Bonferroni's multiple comparison test. Scale bar = 20 µm.

**Figure 7. M1 macrophages and TNF-α level are reduced during the inflammatory phase of wound healing in ITAM receptors-deficient mice.** (A) Detection of macrophages (F4/80$^+$ cells; brown) in wound at day 3 post-injury. (B) Quantification of F4/80$^+$ cells in wound at day 3 post-injury (n=6-8). **p<0.05, **p<0.01.* (C) Comparison of F4/80$^+$ cells between day 1, day 3, and day 9 post-injury in WT and DKO mice. The symbols * and § indicate *p<0.05* in WT and DKO mice, compared to the data at day 1 post-injury, respectively. The bracket shows *p<0.05* for the comparison between day 3 and day 9 post-injury in $^{\S}$DKO mice. Sample numbers at day 1 = 5, day 3 = 6-9, and day 9 post-injury = 10-13, respectively. (D) Immunofluorescence double staining of iNOS (red) and F4/80 (green) in the wound of WT and DKO mice at day 3 (n=4) and day 9 post-injury (n=4). Hoechst counterstains nuclei (blue). (E) Quantification of M1 macrophages (iNOS$^+$F4/80$^+$ cells; yellow) at day 3 post-injury (n=4). **p<0.05.* (F) Quantification of M1 macrophages (iNOS$^+$F4/80$^+$ cells; yellow) at day 9 post-injury (n=4). (G) Immunohistochemistry staining of TNF-α (brown) in the wound at day 3 post-injury. (H) Quantification of TNF-α level in granulation tissue area at day 3 post-injury (n=6). **p<0.05.* Graphs are presented as mean ± SEM and analyzed by either Student's t-test (E, F) or one-way ANOVA with Bonferroni's multiple comparison test (B, C, and H). Scale bar = 20 µm.

**Figure 8. Anti-podoplanin antibody injection in *Gp6*$^{-/-}$ mice (*Gp6*$^{-/-}$ + anti-PDPN) simulates the accelerated phenotype of skin wound repair observed in DKO mice.** (A) Macroscopic appearance of wound at indicated time points. Arrow points to intra-skin bleeding around the wound at day 3 post-injury. (B) Changes of wound size over 3 days post-injury (n=5). (C) H&E staining at day 3 post-injury (n=5). Arrow points the bleeding into surrounding skin. Scale bar = 20 µm. (D) Martius scarlet blue staining of skin wound at day 3 post-injury. Red = old fibrin, blue = collagen, yellow = red blood cells/fresh fibrin. Scale bar = 200 µm. (E) Quantification of fibrin content (red) in the wound at day 3 post-injury (n=5). (F) Staining of neutrophils (Gr-1; brown) in wound area at day 3 post-injury. (G) Quantification of neutrophils (Gr-1$^{+}$ cells) in wound area at day 3 post-injury (n=5). (H) Detection of macrophages (F4/80 staining; brown) in wound area at day 3 post-injury. (I) Quantification of macrophages (F4/80$^{+}$ cells) in wound area at day 3 post-injury (n=5). All graphs are presented as mean ± SEM. Kinetics of wound closure (B) are analyzed by two-way ANOVA with Bonferroni's multiple comparison test. Other parameters are analyzed by Student's t-test. *$p<0.05$.

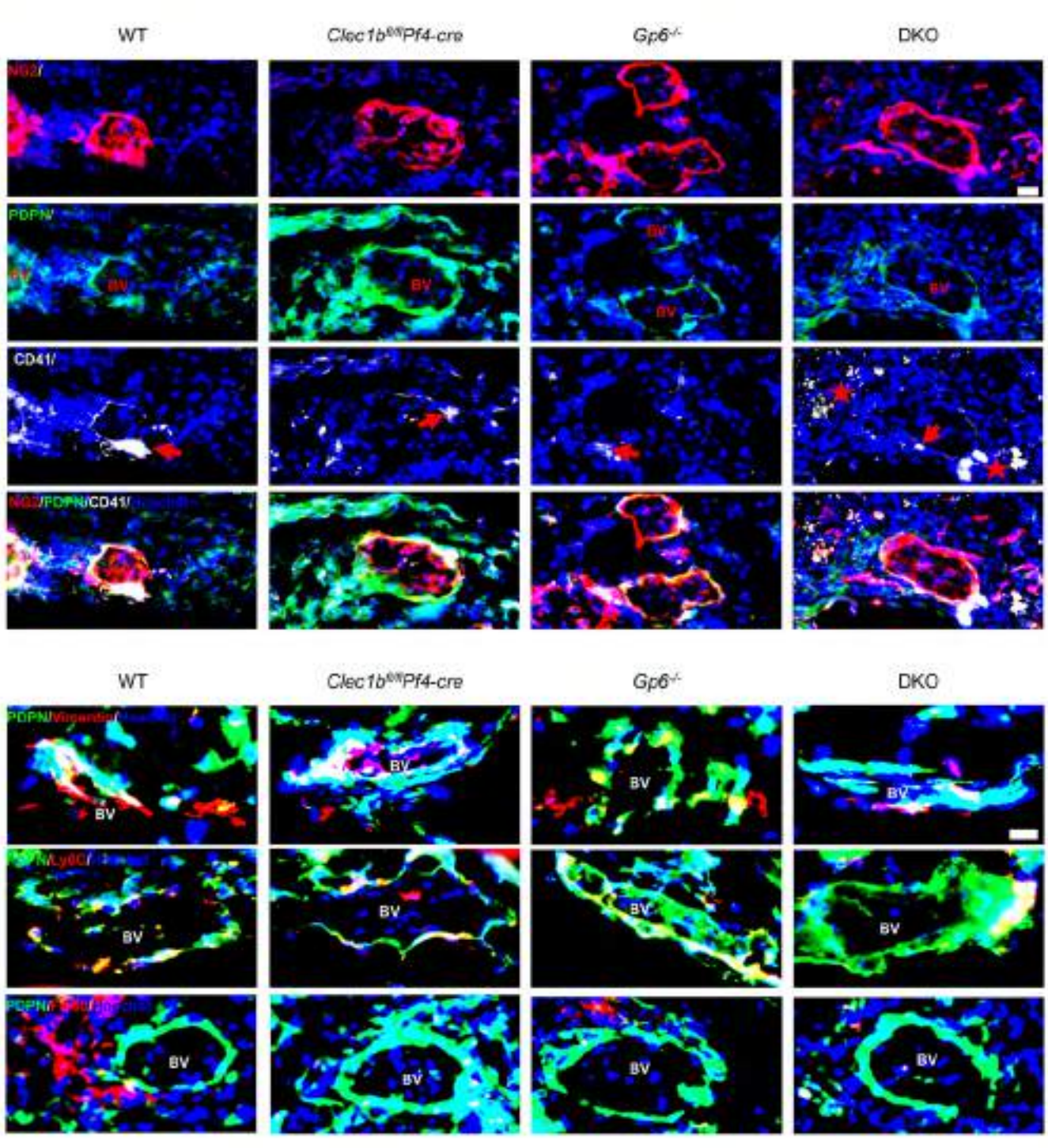
A
WT
Clec1b^fl/fl Pf4-cre
Gp6-/-
DKO
PDPN/
BV
CD41/
PDPN/CD41/
B
WT
Clec1b^fl/fl Pf4-cre
Gp6-/-
DKO
PDPN/
BV

**Figure 1.**

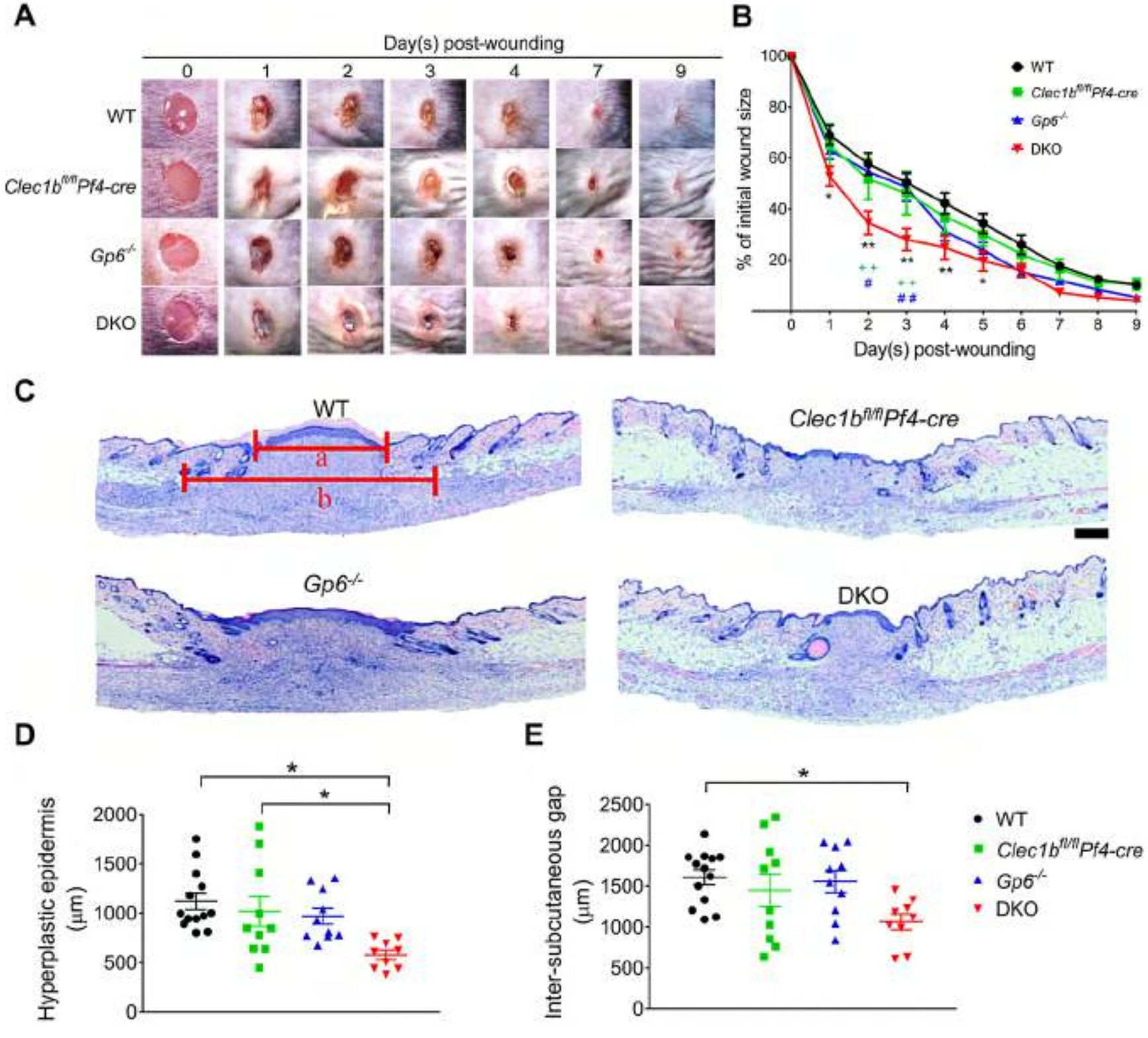
A
Day(s) post-wounding
0
1
2
3
4
7
9
WT
Clec1b^fl/fl Pf4-cre
Gp6^-/-
DKO
B
% of initial wound size
Day(s) post-wounding
WT
Clec1b^fl/fl Pf4-cre
Gp6^-/-
DKO
C
WT
a
b
Clec1b^fl/fl Pf4-cre
Gp6^-/-
DKO
D
Hyperplastic epidermis (μm)
E
Inter-subcutaneous gap (μm)
WT
Clec1b^fl/fl Pf4-cre
Gp6^-/-
DKO

**Figure 2.**

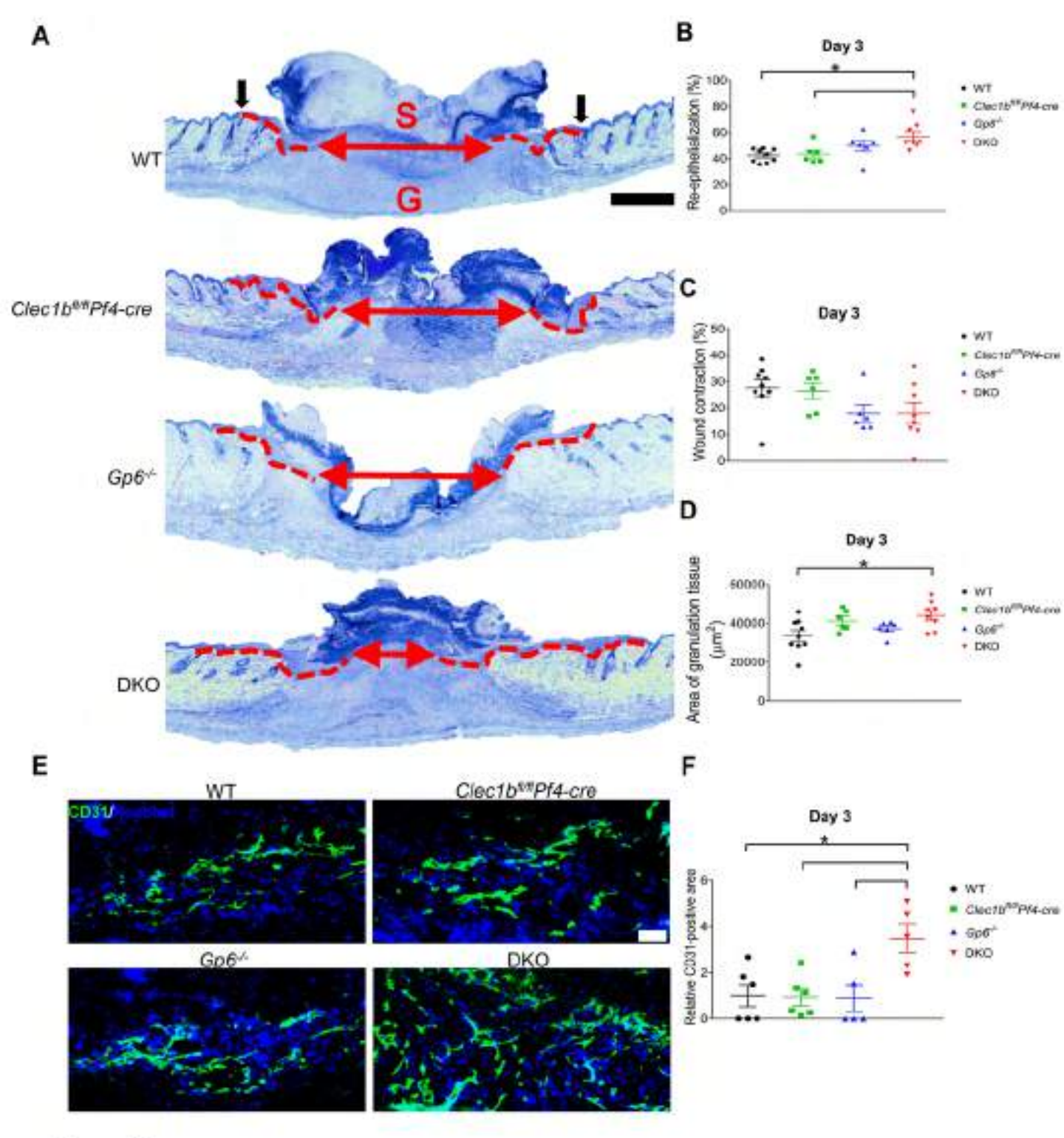
A
WT
S
G
Clec1b^fl/flPf4-cre
Gp6-/-
DKO
B
Day 3
Re-epithelialization (%)
WT
Clec1b^fl/flPf4-cre
Gp6-/-
DKO
C
Day 3
Wound contraction (%)
D
Day 3
Area of granulation tissue (μm²)
E
WT
Clec1b^fl/flPf4-cre
CD31
Gp6-/-
DKO
F
Day 3
Relative CD31-positive area

**Figure 3.**

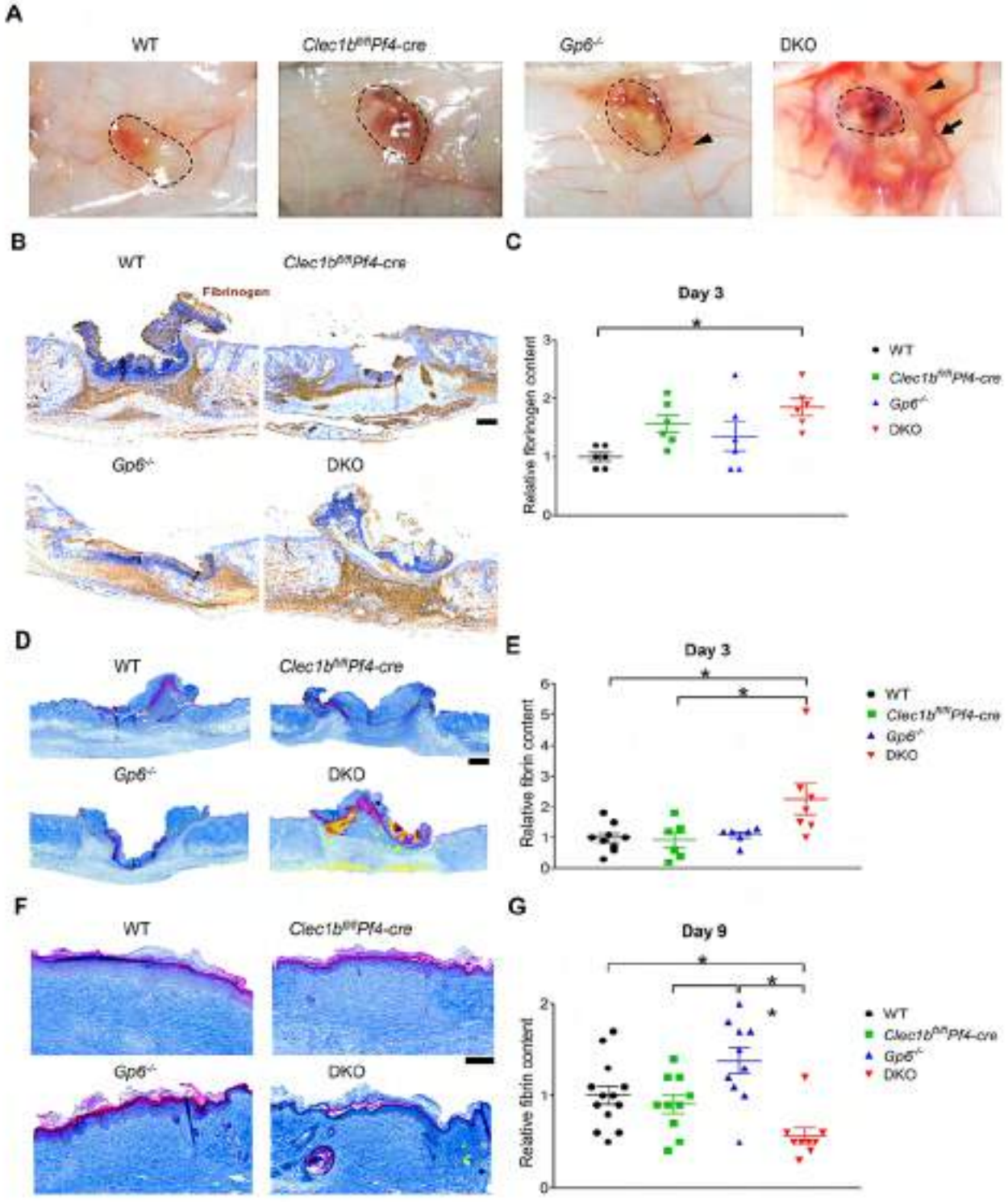
A
WT
Clec1b^fl/flPf4-cre
Gp6-/-
DKO
B
WT
Clec1b^fl/flPf4-cre
Fibrinogen
Gp6-/-
DKO
C
Day 3
Relative fibrinogen content
WT
Clec1b^fl/flPf4-cre
Gp6-/-
DKO
D
WT
Clec1b^fl/flPf4-cre
Gp6-/-
DKO
E
Day 3
Relative fibrin content
WT
Clec1b^fl/flPf4-cre
Gp6-/-
DKO
F
WT
Clec1b^fl/flPf4-cre
Gp6-/-
DKO
G
Day 9
Relative fibrin content
WT
Clec1b^fl/flPf4-cre
Gp6-/-
DKO

**Figure 4.**

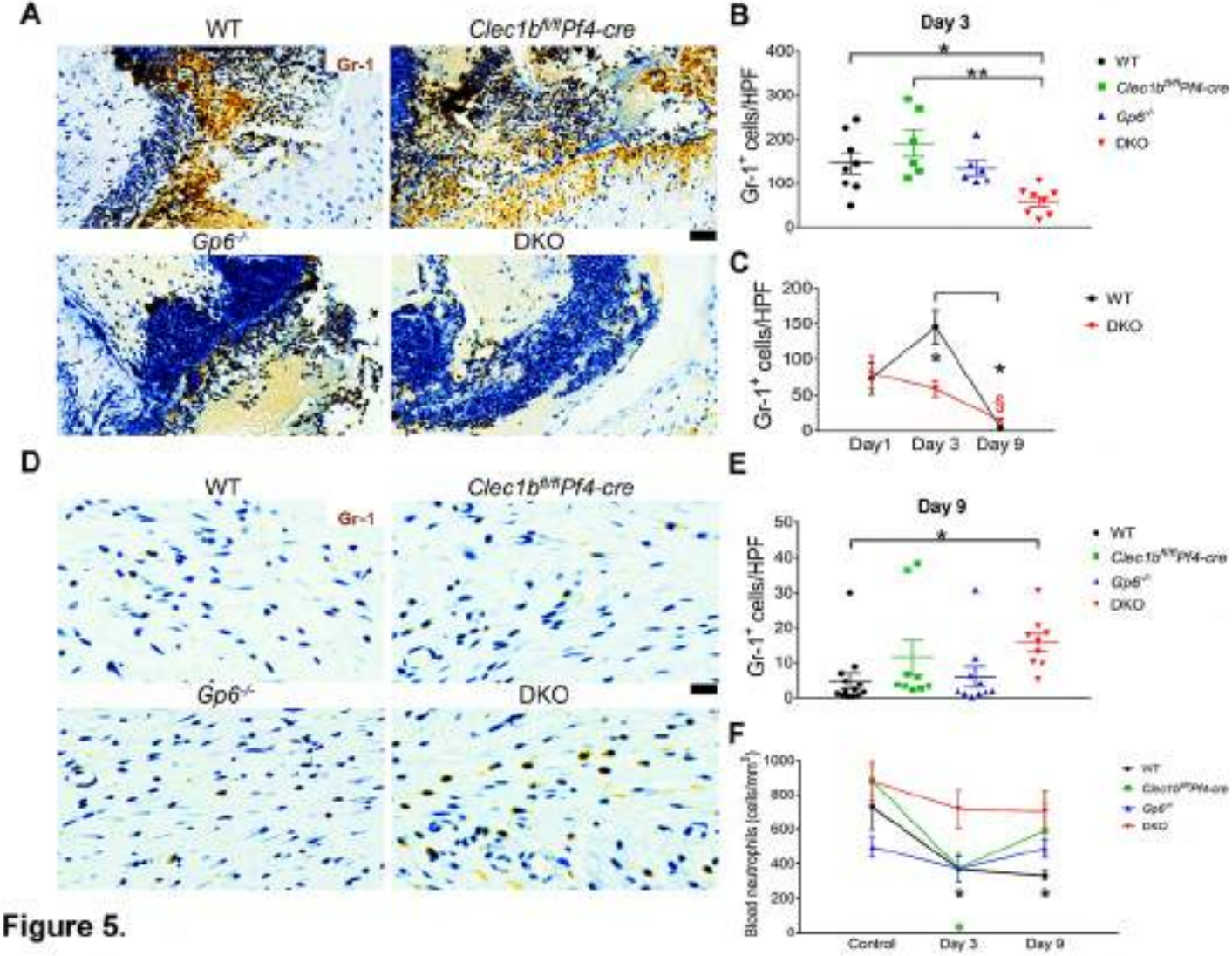
A
WT
Clec1b^fl/fl Pf4-cre
Gr-1
Gp6^-/-
DKO
B
Day 3
Gr-1+ cells/HPF
WT
Clec1b^fl/fl Pf4-cre
Gp6^-/-
DKO
C
Gr-1+ cells/HPF
WT
DKO
Day1
Day 3
Day 9
D
WT
Clec1b^fl/fl Pf4-cre
Gr-1
Gp6^-/-
DKO
E
Day 9
Gr-1+ cells/HPF
WT
Clec1b^fl/fl Pf4-cre
Gp6^-/-
DKO
F
Blood neutrophils (cells/mm3)
WT
Clec1b^fl/fl Pf4-cre
Gp6^-/-
DKO
Control
Day 3
Day 9

**Figure 5.**

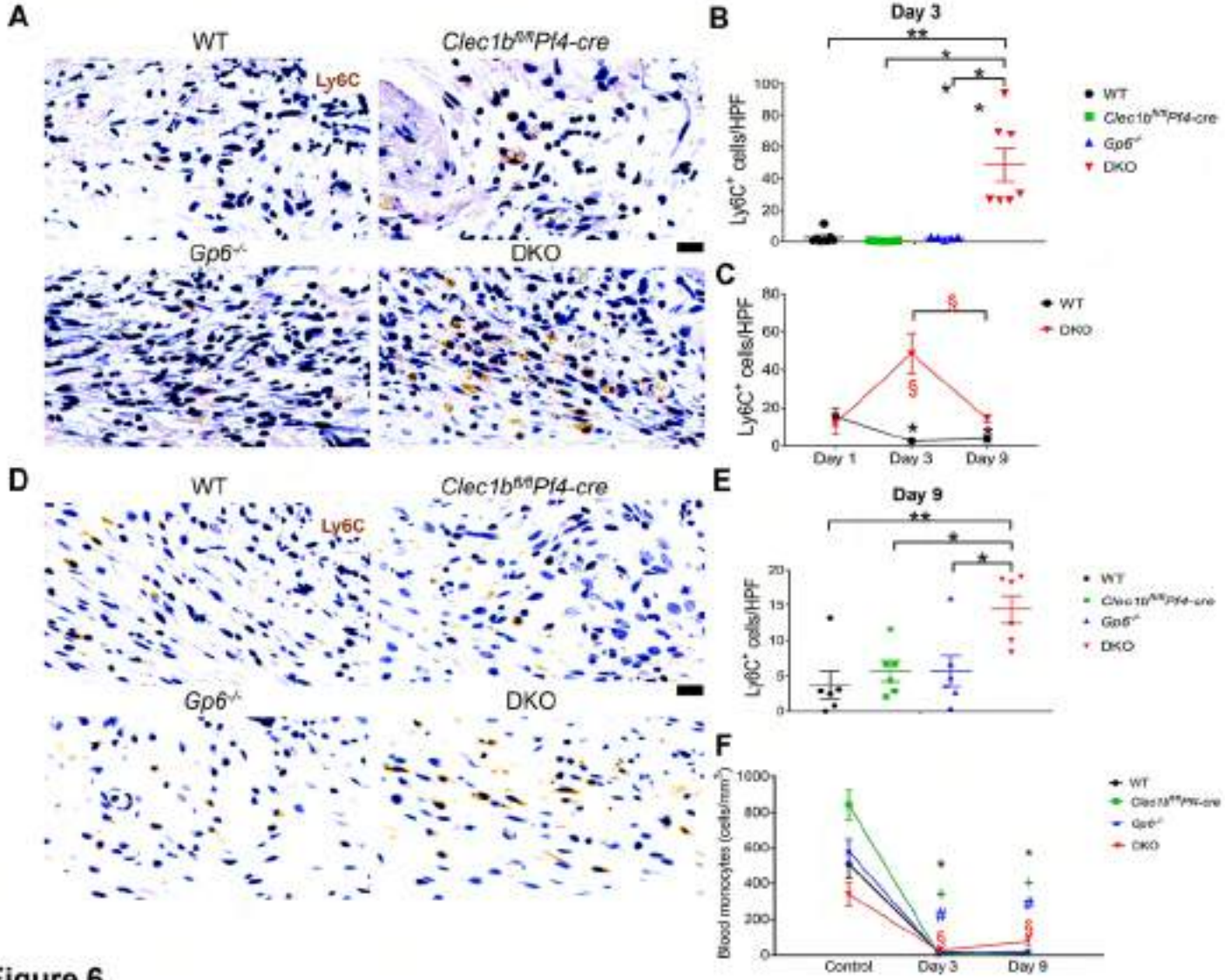
A
WT
Clec1b^fl/fl Pf4-cre
Ly6C
Gp6^-/-
DKO
B
Day 3
Ly6C+ cells/HPF
WT
Clec1b^fl/fl Pf4-cre
Gp6^-/-
DKO
C
Ly6C+ cells/HPF
Day 1
Day 3
Day 9
D
E
Day 9
F
Blood monocytes (cells/mm3)
Control

**Figure 6.**

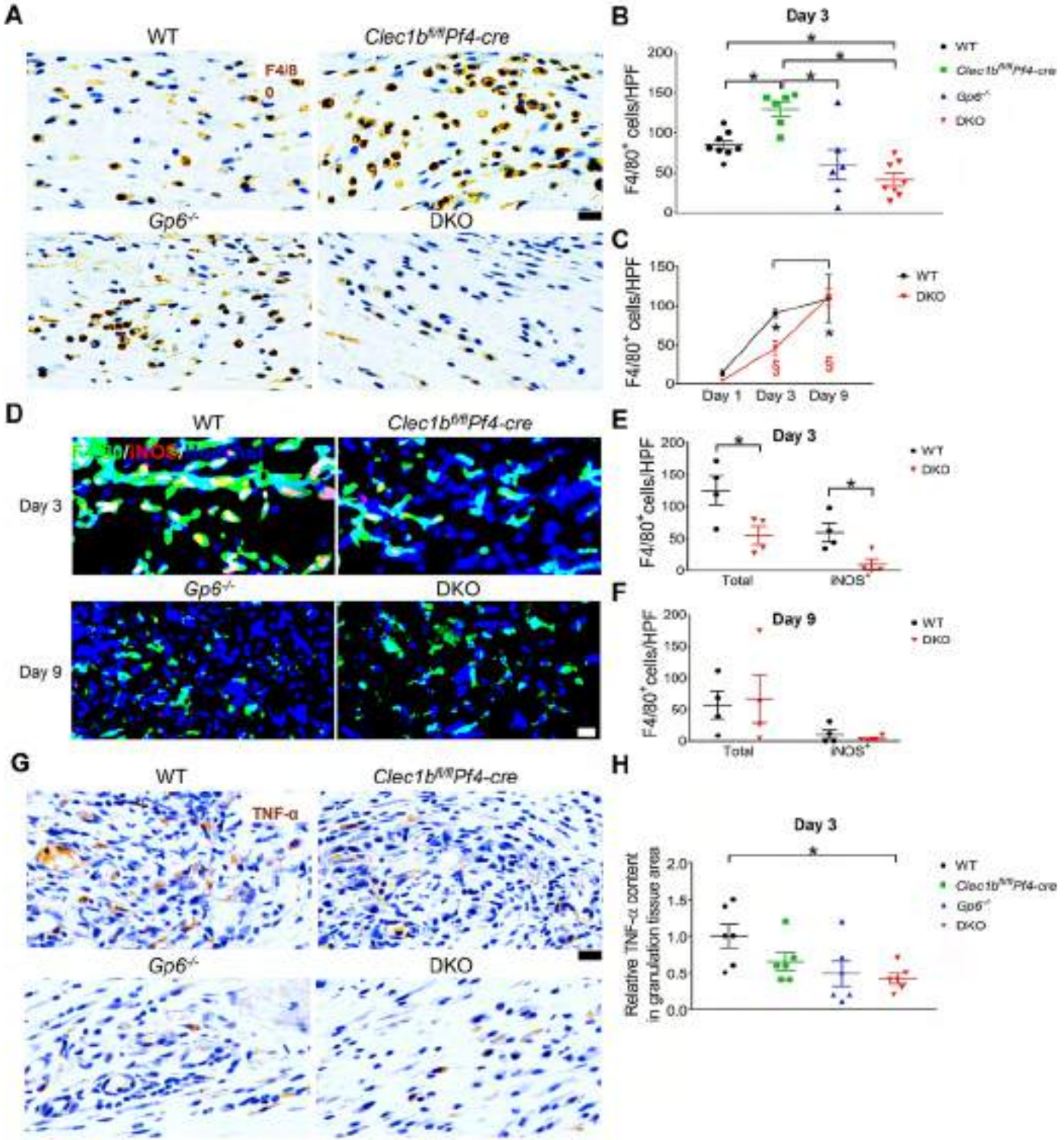
A
WT
Clec1b^fl/fl Pf4-cre
F4/8
0
Gp6^-/-
DKO
B
Day 3
F4/80+ cells/HPF
WT
Clec1b^fl/fl Pf4-cre
Gp6^-/-
DKO
C
F4/80+ cells/HPF
Day 1
Day 3
Day 9
WT
DKO
D
WT
Clec1b^fl/fl Pf4-cre
Day 3
Gp6^-/-
DKO
Day 9
E
Day 3
F4/80+cells/HPF
Total
iNOS+
WT
DKO
F
Day 9
F4/80+cells/HPF
Total
iNOS+
WT
DKO
G
WT
Clec1b^fl/fl Pf4-cre
TNF-α
Gp6^-/-
DKO
H
Day 3
Relative TNF-α content in granulation tissue area
WT
Clec1b^fl/fl Pf4-cre
Gp6^-/-
DKO

**Figure 7.**

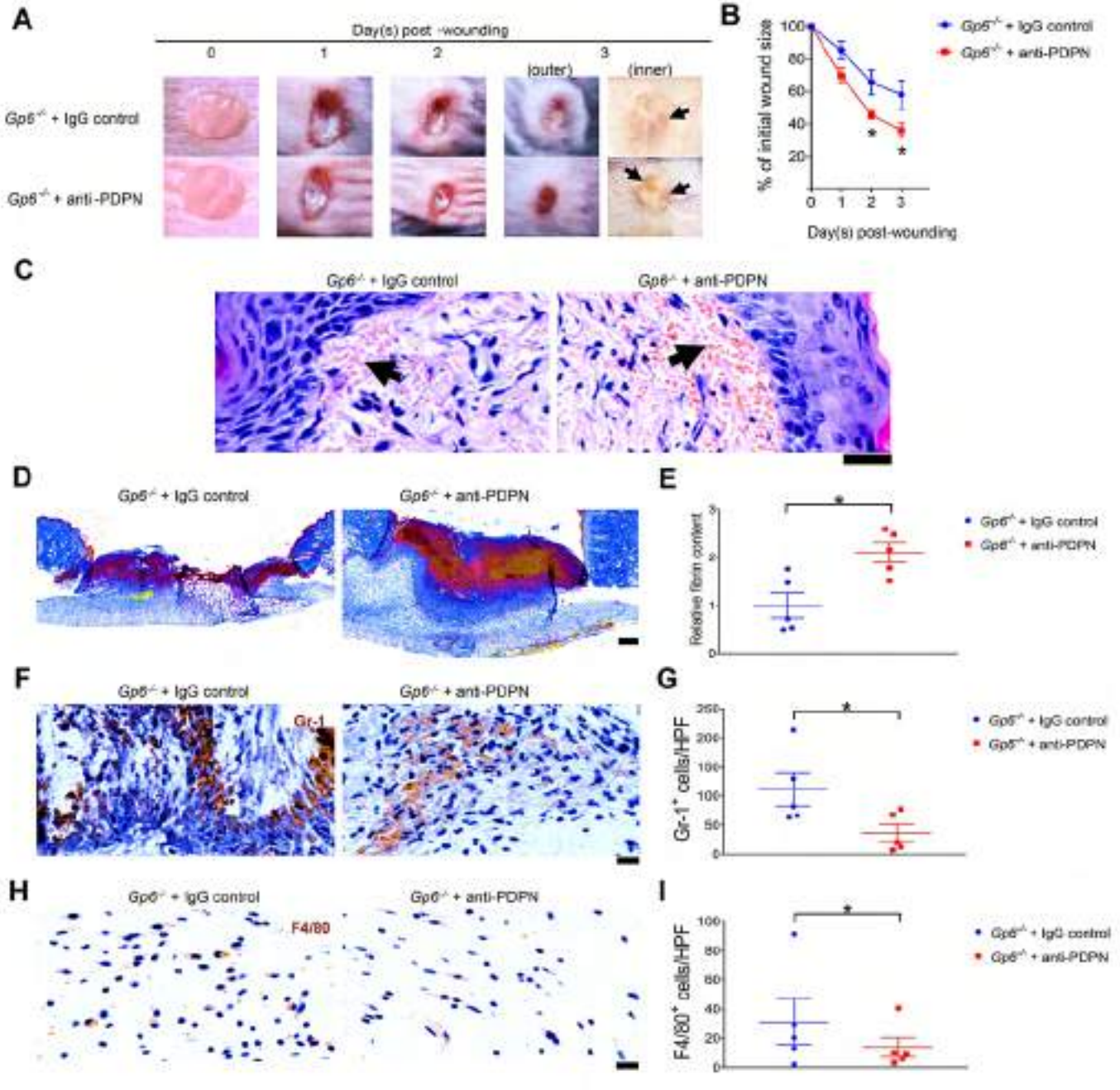
A
Day(s) post -wounding
0
1
2
3
(outer)
(inner)
Gp6-/- + IgG control
Gp6-/- + anti-PDPN
B
% of initial wound size
Day(s) post-wounding
Gp6-/- + IgG control
Gp6-/- + anti-PDPN
C
Gp6-/- + IgG control
Gp6-/- + anti-PDPN
D
Gp6-/- + IgG control
Gp6-/- + anti-PDPN
E
Relative fibrin content
Gp6-/- + IgG control
Gp6-/- + anti-PDPN
F
Gp6-/- + IgG control
Gp6-/- + anti-PDPN
Gr-1
G
Gr-1+ cells/HPF
Gp6-/- + IgG control
Gp6-/- + anti-PDPN
H
Gp6-/- + IgG control
Gp6-/- + anti-PDPN
F4/80
I
F4/80+ cells/HPF
Gp6-/- + IgG control
Gp6-/- + anti-PDPN

**Figure 8.**

**Supplemental materials**

**Supplemental methods:**

## Animal

In this study, C57BL/6 mice were bred to produce wild type (WT) and platelet-specific CLEC-2-deficient (*Clec1b*$^{fl/fl}$*Pf4-Cre*)[1] mice as littermates separately from GPVI knockout (*Gp6*$^{-/-}$)[2] and CLEC-2/GPVI double-deficient (*Clec1b*$^{fl/fl}$*Pf4-Cre/Gp6*$^{-/-}$; DKO) mice. Additionally, *Clec1b*$^{fl/fl}$*Pf4-Cre* mice were used for breeding in the DKO producing colony. Cross comparisons were made between related, age- and sex-matched animals to control natural variation between mouse strains, including between WT and DKO mice.

## Morphometric analysis

Wounds were excised, fixed in 4% paraformaldehyde and processed using a standard paraffin embedding protocol. Paraffin-embedded skin samples (5 μm) were used for hematoxylin and eosin (H&E) staining. Tissues were imaged using a ZEISS AxioScan.Z1 slide scanner. As shown in the scheme below, the proliferation of keratinocytes forms the hyperplastic epidermis (He) at the wound edge within a few days after injury. The granulation tissue, containing newly formed blood vessels, infiltrating cells, and molecules, is also formed to facilitate wound healing. Keratinocytes migrate underneath the scab and above the granulation tissue, which generate epithelial tongues toward the centre of the wound to resurface skin epidermis (the tips of epithelial tongue are indicated by red arrow).[3-5] Morphometric analysis of skin histology was performed manually using a freehand line tool in Fiji (a distribution of ImageJ software)[6], and the terms were defined in the following ways;

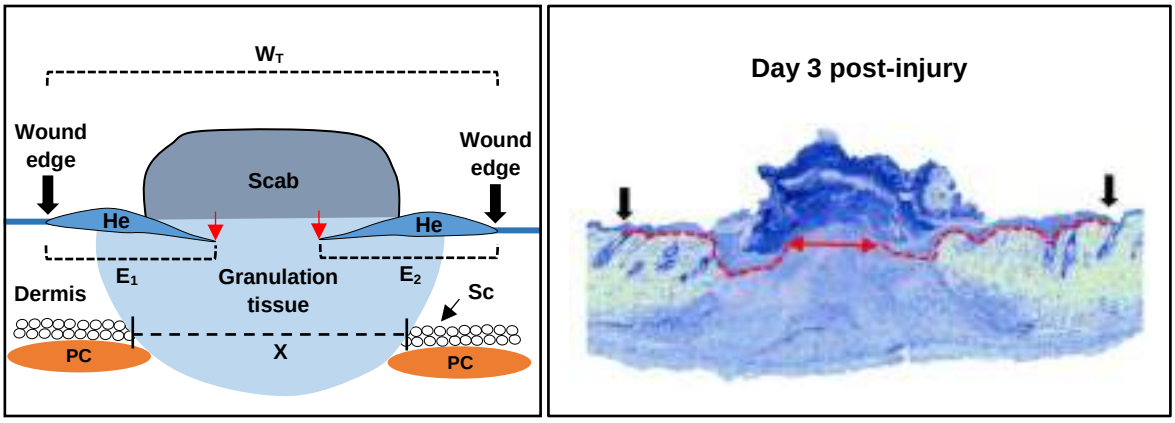


- Re-epithelialization is the re-generation of skin epidermis.[7,8] The area of thickening keratinocytes immediately next to the normal skin in histology images is considered as the wound edge for measuring re-epithelialization.[8-13] Percentage of re-epithelialization at day 3 post-injury was calculated using the formula[8,9];

$$\% \text{ Re-epithelialization} = [(E_1+E_2)/W_0] \times 100$$

where $E_1$ and $E_2$ = distance of epithelial tongue from each side of wound edge

$W_0$ = original wound diameter at day 0

- Wound contraction, which is mediated by the specialized muscle called "*panniculus carnosus* (PC)" in deeper layer of murine skin, also affects wound closure.[14] To exclude the influence of this effect, closure by contraction at day 3 post-injury was calculated using the formula[9];

$$\% \text{ Wound contraction} = [(W_0-W_T)/W_0] \times 100$$

where $W_T$ = distance between the wound edges at indicated time point

- The area of granulation tissue, which contributes to new tissue re-formation, was also measured at day 3 post-injury.[4,5]
- Following the complete wound closure, thickened layer of keratinocytes is remained, known as scar. Thus, the length of hyperplastic epidermis ("a" in Figure 2C), which indicates the size of scar at upper layer, was examined at day 9 post-injury.[5,15]
- Measurement of distance between intact subcutaneous (Sc) edges at both side of the wound ("X" in above scheme and "b" in Figure 2C), which represents the size of scar in the deeper layer, was also performed at day 9 post-injury.[5]

**Measurement of fibrin and collagen contents**

Martius scarlet blue staining (Atom Scientific, UK) was used to detect fibrin and collagen. High power field (HPF) images were taken from the whole wound area. To calculate the mean intensity, the fibrin (red color) and collagen signals (blue color) were isolated using the Fiji Colour Deconvolution plugin (Masson Trichrome)[16] and the threshold set using the Otsu method[17]. A total intensity was normalized by total measured area, and expressed as fold relative to WT.

**Immunohistochemistry and immunofluorescence**

Immunohistochemistry staining for Gr-1, Ly6C, F4/80, fibrinogen, tissue factor (TF), tumor necrosis factor (TNF)-α, platelet factor 4 (PF4), CXCL-1 and podoplanin were performed on paraffin-embedded skin section (5 μm) according to a standard protocol[18]; horseradish peroxidase (HRP)-conjugated secondary antibodies and ImpactDAB substrate (SK-4105, Vector Lab) were used for signal detection. HPF images were taken from the whole wound area. Brown color was separated using IHC toolbox in

Fiji then thresholded (Otsu). The binary images were processed by filling holes and a watershed transform to separate touching cells. Per cell measurements were calculated for all connected areas larger than 45 square microns. Gr-1$^+$, Ly6C$^+$ and F4/80$^+$ cells were counted and presented per HPF[19], while intensity of TF[20], TNF-α, PF4, and CXCL-1[21] were quantified and normalized by total measured area, then expressed as fold relative to wild-type (WT).

Immunofluorescence staining for neuron-glial antigen 2 (NG2), CD41, podoplanin, vimentin, Ly6C, Ly6G, iNOS, Fizz-1, F4/80, and CD31 were processed in optimal cutting temperature compound (O.C.T)-embedded frozen skin sections (10 μm). Fluorophore-conjugated secondary antibodies were used to detect signals. Hoechst (H3570, Life Technologies) was used to stain nuclei. HPF images were taken from the whole wound area. CD31$^+$ area[22] was calculated using Otsu thresholding (Fiji) and normalized by total measured area, and presented as fold relative to WT. The iNOS$^+$F4/80$^+$ cells and Fizz-1$^+$F4/80$^+$ cells were counted using Fiji according to the previous protocol[23] with adaptation. In brief, HPF image of either iNOS$^+$F4/80$^+$ or Fizz-1$^+$F4/80$^+$ double staining was split into a single blue (nuclei), green (F4/80) and red (iNOS or Fizz-1) channel, respectively. The threshold of green fluorescence was set using Otsu model. Then, the binary images were processed by a watershed to separate attached particles. The red fluorescence was also thresholded. To create a merged image of previously processed red and green channels, the “image calculator” mode from process menu was used, followed by choosing the operator “AND”. Finally, all connected areas larger than 45 square microns were counted as per cell measurements. The antibodies used are described in Table S1.

**In vitro neutrophil migration assay**

Neutrophils were isolated from the bone marrow of WT or DKO mice as previously described[24] and purity was checked using anti-Ly6G antibody. Isolated neutrophils (50,000 cells diluted in Hank's Balanced Salt Solution + 0.5 % bovine serum albumin) were loaded into the upper well of a chemotaxis chip (Ibidis). The chemotaxis chips were coated with collagen (10µg/ml), fibrinogen (100 µg/ml) or crosslinked fibrin (prepared by mixing fibrinogen (1 mg/ml), thrombin (1 U/ml), $Ca^{2+}$ (10 mM), and FXIIIa (7 µg/ml) in PBS for 1 hour at 37 °C). Chemotaxis toward fMLP (5 µM, Sigma) was assessed for 3 hours. After fixation with formalin, the cells in the loaded and migrated wells were imaged, and the number of cells in five representative areas per sample was quantified using Fiji. Finally, percentage of migrated cells was calculated using the formula;

$$\text{Percent neutrophil migration} = [N1/(N1+N2)] \times 100$$

Where N1 = numbers of migrated cells, N2 = numbers of remaining cells in loaded chamber

**Hematological analysis**

Whole blood was collected from the inferior vena cava using ethylenediaminetetraacetic acid (EDTA)-filled syringe. Blood counts were analyzed on an ABX Pentra 60 (Horbia Ltd, UK).

**Statistical analysis**

All data are presented as mean ± standard error of mean (SEM). Two-way ANOVA with Bonferroni's multiple comparison test was used to compare kinetics of wound closure. Mean differences in other parameters were analyzed by either Student's t-test (two groups comparison) or one-way ANOVA with Bonferroni post-hoc test (more than two groups) using GraphPad Prism software. $p<0.05$ was considered as statistically significant.

## Table S1. List of antibodies used in immunostaining

| Reagents | Working dilution | Company | Cat No. |
|---|---|---|---|
| ***Primary antibodies*** | | | |
| Rat anti-mouse Gr-1 monoclonal antibody | 1:200 | eBiosciences | 14-5931-82 |
| Rat anti-mouse F4/80 monoclonal antibody | 1:200 (IHC)<br>1:100 (IF) | Bio-Rad | MCA497GA |
| Rabbit anti-mouse CXCL-1 monoclonal antibody | 1:200 | R&D systems | MAB4532 |
| Syrian hamster anti-mouse podoplanin monoclonal antibody | 1:500 (IHC)<br>1:200 (IF) | eBiosciences | 14-5381-85 |
| Rat anti-mouse CD41 monoclonal antibody | 1:100 | BD Pharmagen | 553847 |
| Rabbit anti-CD31 polyclonal antibody | 1:100 | Abcam | ab28364 |
| Rabbit anti-NG2 chondroitin sulfate proteoglycan polyclonal antibody | 1:200 | Merk Millipore | AB5320 |
| Rabbit anti-tissue factor monoclonal antibody | 1:400 | Abcam | ab151748 |
| Rabbit anti-TNF alpha polyclonal antibody | 1:200 | Abcam | ab9739 |
| Rat anti-mouse Ly6C monoclonal antibody | 1:200 | Biolegend | 128002 |
| Rat anti-mouse CXCL4/PF4 monoclonal antibody | 1:200 | R&D systems | MAB595-100 |
| Goat anti-mouse fibrinogen polyclonal antibody | 1:200 | Accurate Chemical & Scientific Corp. | YNGMFBG7S |
| Rabbit anti-vimentin monoclonal antibody | 1:200 | R&D systems | MAB2105 |
| Rabbit anti-iNOS polyclonal antibody | 1:50 | Abcam | ab15323 |
| Rabbit anti-RELM alpha (Fizz-1) polyclonal antibody | 1:50 | Abcam | ab39626 |
| Rat anti-mouse Ly6G-APC/Cy7-conjugated monoclonal antibody (clone 1A8) | 1:100 | BD Pharmagen | 560600 |
| ***IgG control*** | | | |
| Rat IgG2b control | 1:400 | Bio-Rad | MCA1125 |
| Rat IgG1,K control | 1:200 | Biolegend | 400402 |
| Golden Syrian hamster IgG control | 1:500 (IHC)<br>1:200 (IF) | eBiosciences | 14-4914-85 |
| Rabbit IgG control | 1: 10,000 | Life technologies | 10500C |
| ***Secondary antibodies*** | | | |
| Goat anti-rat IgG-HRP | 1:200 (Gr-1)<br>1:500 (F4/80) | Santa Cruz | sc-2032 |
| Goat anti-hamster IgG-HRP | 1:500 | Santa Cruz | sc-2905 |
| Donkey anti-rabbit IgG-HRP | 1:200 | GE Healthcare | NA934V |
| Donkey anti-goat IgG-HRP | 1:500 | Santa Cruz | Sc-2020 |
| Goat anti-rat IgG-Alexa 568 | 1:200 | Life technologies | A11077 |
| Goat anti-rat IgG-Alexa 488 | 1:200 (vimentin)<br>1:100 (F4/80) | Life technologies | A11006 |
| Goat anti-hamster IgG-Alexa 488 | 1:200 | Life technologies | A21110 |
| Goat anti-rabbit IgG-Alexa 647 | 1:200<br>1:100 (iNOS and Fizz-1) | Life technologies | A21245 |
| Hoechst | 1:10,000 | Life technologies | H3570 |

IHC = Immunohistochemistry, IF = Immunofluorescence

**References**


1. Finney BA, Schweighoffer E, Navarro-Nunez L, et al. CLEC-2 and Syk in the megakaryocytic/platelet lineage are essential for development. Blood. 2012;119(7):1747-1756.
2. Kato K, Kanaji T, Russell S, et al. The contribution of glycoprotein VI to stable platelet adhesion and thrombus formation illustrated by targeted gene deletion. Blood. 2003;102(5):1701-1707.
3. Shaw TJ, Martin P. Wound repair at a glance. J Cell Sci. 2009;122(Pt 18):3209-3213.
4. Lucas T, Waisman A, Ranjan R, et al. Differential roles of macrophages in diverse phases of skin repair. J Immunol. 2010;184(7):3964-3977.
5. Yang HS, Shin J, Bhang SH, et al. Enhanced skin wound healing by a sustained release of growth factors contained in platelet-rich plasma. Exp Mol Med. 2011;43(11):622-629.
6. Schindelin J, Arganda-Carreras I, Frise E, et al. Fiji: an open-source platform for biological-image analysis. Nat Methods. 2012;9(7):676-682.
7. Ben Amar M, Wu M. Re-epithelialization: advancing epithelium frontier during wound healing. J R Soc Interface. 2014;11(93):20131038.
8. Stavrou EX, Fang C, Bane KL, et al. Factor XII and uPAR upregulate neutrophil functions to influence wound healing. J Clin Invest. 2018;128(3):944-959.
9. Chen L, Mirza R, Kwon Y, DiPietro LA, Koh TJ. The murine excisional wound model: Contraction revisited. Wound Repair Regen. 2015;23(6):874-877.
10. Oda Y, Hu L, Nguyen T, Fong C, Tu CL, Bikle DD. Combined Deletion of the Vitamin D Receptor and Calcium-Sensing Receptor Delays Wound Re-epithelialization. Endocrinology. 2017;158(6):1929-1938.
11. Sheets AR, Demidova-Rice TN, Shi L, Ronfard V, Grover KV, Herman IM. Identification and Characterization of Novel Matrix-Derived Bioactive Peptides: A Role for Collagenase from Santyl(R) Ointment in Post-Debridement Wound Healing? PLoS One. 2016;11(7):e0159598.
12. Carretero M, Escamez MJ, Garcia M, et al. In vitro and in vivo wound healing-promoting activities of human cathelicidin LL-37. J Invest Dermatol. 2008;128(1):223-236.
13. Schmidt BA, Horsley V. Intradermal adipocytes mediate fibroblast recruitment during skin wound healing. Development. 2013;140(7):1517-1527.

14. Davidson JM, Yu F, Opalenik SR. Splinting Strategies to Overcome Confounding Wound Contraction in Experimental Animal Models. Adv Wound Care (New Rochelle). 2013;2(4):142-148.
15. Rono B, Engelholm LH, Lund LR, Hald A. Gender affects skin wound healing in plasminogen deficient mice. PLoS One. 2013;8(3):e59942.
16. Ruifrok AC, Johnston DA. Quantification of histochemical staining by color deconvolution. Anal Quant Cytol Histol. 2001;23(4):291-299.
17. Luo TL, Eisenberg MC, Hayashi MAL, et al. A Sensitive Thresholding Method for Confocal Laser Scanning Microscope Image Stacks of Microbial Biofilms. Sci Rep. 2018;8(1):13013.
18. Ramos-Vara JA. Principles and Methods of Immunohistochemistry. Methods Mol Biol. 2017;1641:115-128.
19. Qiang L, Sample A, Liu H, Wu X, He YY. Epidermal SIRT1 regulates inflammation, cell migration, and wound healing. Sci Rep. 2017;7(1):14110.
20. Zhou J, May L, Liao P, Gross PL, Weitz JI. Inferior vena cava ligation rapidly induces tissue factor expression and venous thrombosis in rats. Arterioscler Thromb Vasc Biol. 2009;29(6):863-869.
21. Smith E, Prasad KM, Butcher M, et al. Blockade of interleukin-17A results in reduced atherosclerosis in apolipoprotein E-deficient mice. Circulation. 2010;121(15):1746-1755.
22. Uchiyama A, Yamada K, Ogino S, et al. MFG-E8 regulates angiogenesis in cutaneous wound healing. Am J Pathol. 2014;184(7):1981-1990.
23. Arqués O, Chicote I, Tenbaum S, Puig I, Palmer HG. Standardized Relative Quantification of Immunofluorescence Tissue Staining. Protocol Exchange 2012.
24. Swamydas M, Lionakis MS. Isolation, purification and labeling of mouse bone marrow neutrophils for functional studies and adoptive transfer experiments. J Vis Exp. 2013(77):e50586.

**Supplemental Figures:**

**Figure S1**

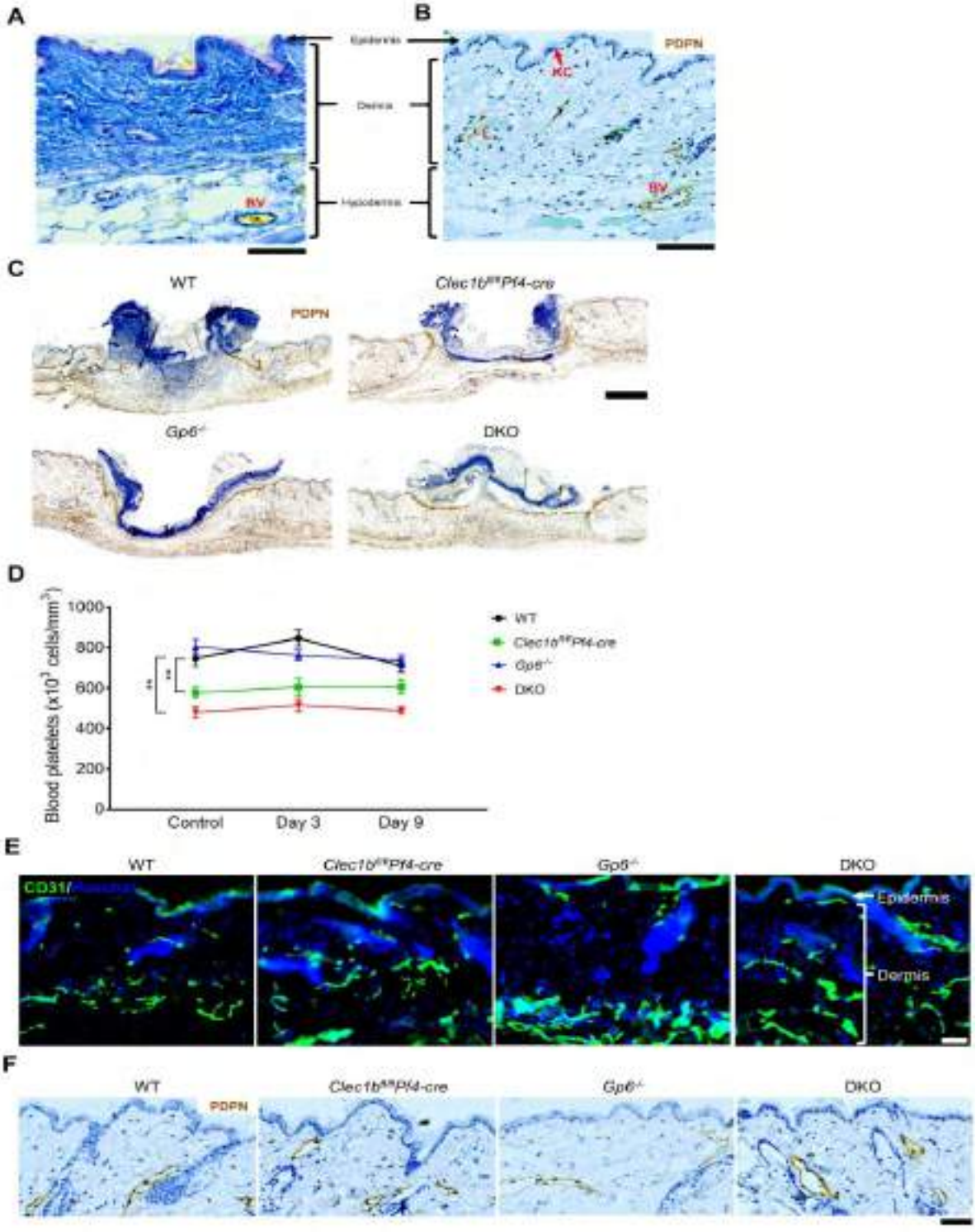

**Figure S1. Platelet CLEC-2 deficient mice and DKO mice have lower baseline platelet counts than WT but no alteration in density of blood and lymphatic vessels in skin tissues.** (A) Martius scarlet blue (MSB) staining shows collagen (blue) in dermis and hypodermis of unchallenged WT mouse skin (n=5). Red = old fibrin, blue = collagen, yellow = red blood cells/fresh fibrin. Scale bar = 100 μm. (B) Immunohistochemistry of podoplanin (brown) in unchallenged WT mouse skin (n=5). L = lymphatic vessel, KC = keratinocyte. PDPN = podoplanin. BV = blood vessel. Scale bar = 100 μm. (C) Podoplanin immunohistochemistry staining (brown) of skin wound at day 3 post-injury shows upregulation of podoplanin on migrating keratinocytes and on stromal and infiltrating cells within the granulation tissue in all groups (n=6-9). Scale bar = 500 μm. (D) Comparison of platelet counts between baseline, day 3, and day 9 post-injury in each mouse strain. Sample numbers (n) at baseline = 10, day 3 post-injury = 6-9, and day 9 post-injury = 10-13, respectively. *$**p<0.01$*. (E) Immunofluorescence staining of CD31 (green) in unchallenged skin of WT and genetically modified mice (n=5). Hoechst counterstains nuclei (blue). Scale bar = 50 μm. (F) Immunohistochemistry staining shows podoplanin (brown) on lymphatic vessels in unchallenged skin of WT and genetically modified mice (n=5). PDPN = podoplanin. Scale bar = 50 μm.

**Figure S2**

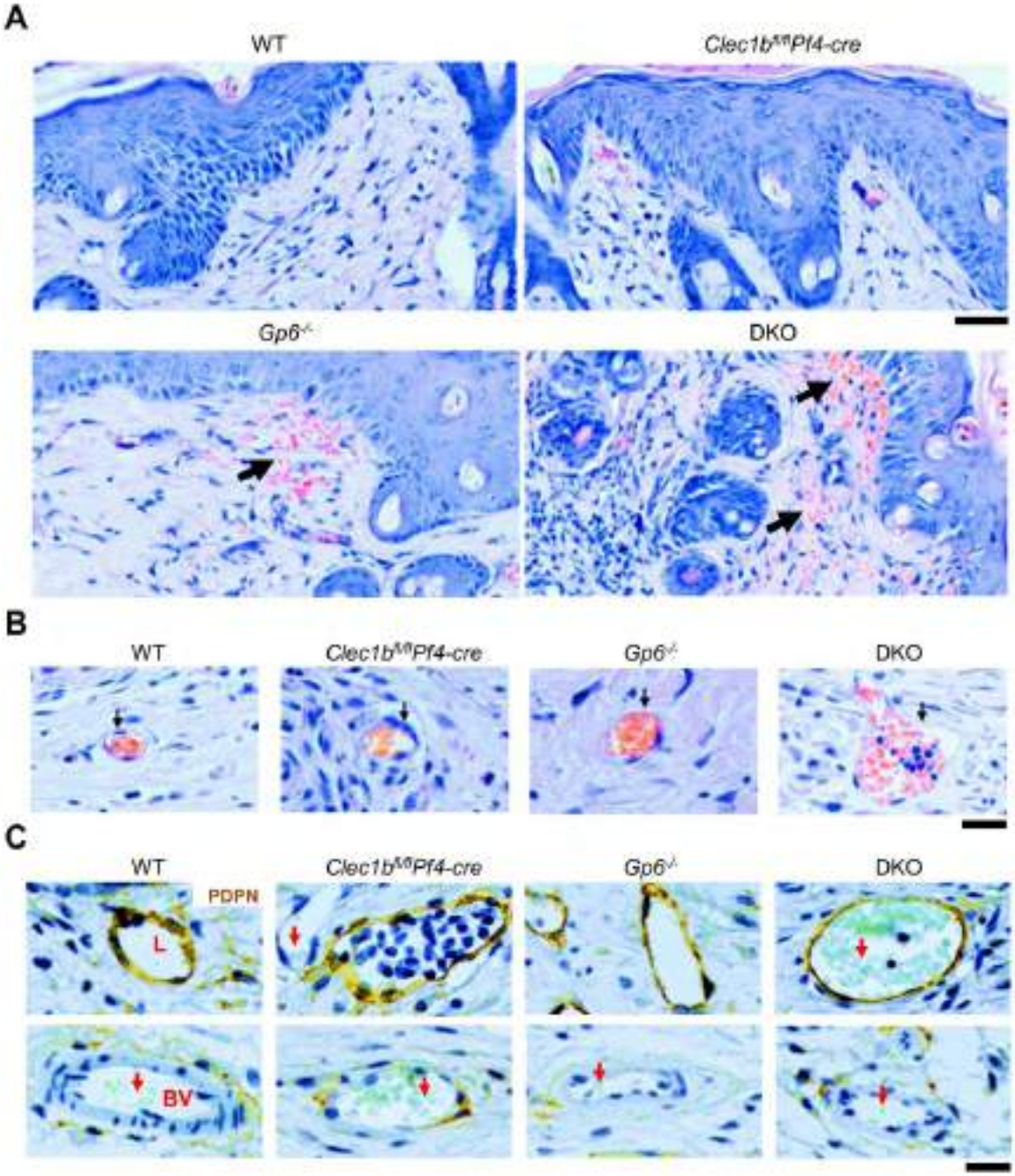
A
WT
Clec1b^fl/flPf4-cre
Gp6-/-
DKO
B
WT
Clec1b^fl/flPf4-cre
Gp6-/-
DKO
C
WT
Clec1b^fl/flPf4-cre
Gp6-/-
DKO
PDPN
L
BV

**Figure S2. Vascular leakage is observed in DKO mice and less marked in *Gp6*$^{-/-}$ mice during the inflammatory phase of wound healing.** (A) H&E staining of wounds at day 3 post-injury (n=6-9). Arrow indicates bleeding into surrounding skin. Scale bar = 50 µm. (B) H&E staining of wound scar at day 9 post-injury (n=10-13). Arrow indicates red blood cells within the vessel. Scale bar = 20 µm. (C) Immunohistochemistry shows podoplanin on lymphatic endothelium (upper panel) and cells around blood vessel (lower panel). L = lymphatic vessel. BV = blood vessel. Arrow points to red blood cells in both types of vasculature. Scale bar = 20 µm.

**Figure S3**

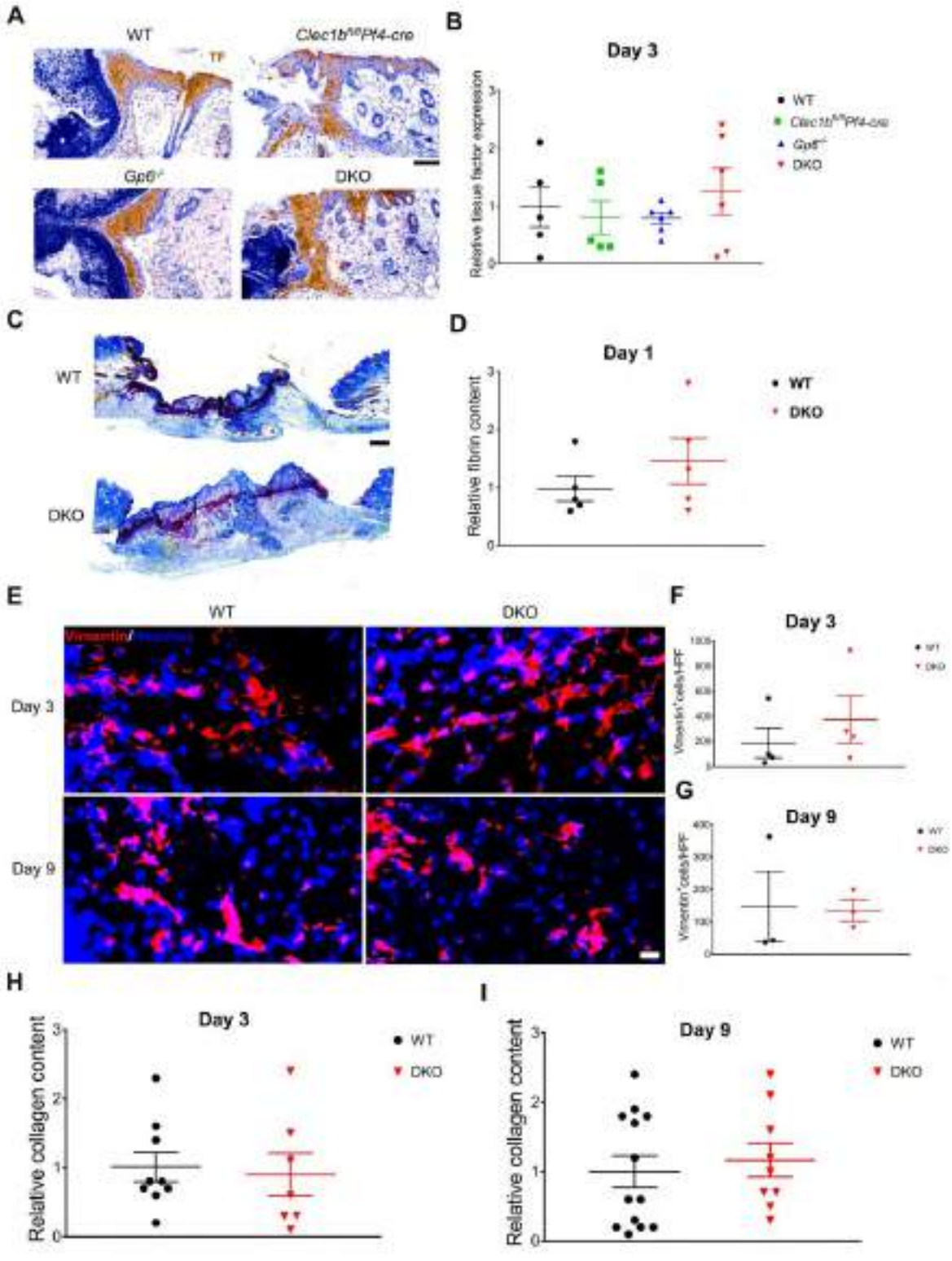
A
WT
Clec1b^fl/fl PF4-cre
TF
Gp6^-/-
DKO
B
Day 3
Relative tissue factor expression
WT
Clec1b^fl/fl PF4-cre
Gp6^-/-
DKO
C
WT
DKO
D
Day 1
Relative fibrin content
WT
DKO
E
WT
DKO
Vimentin/
Day 3
Day 9
F
Day 3
Vimentin+cells/HPF
G
Day 9
Vimentin+cells/HPF
H
Day 3
Relative collagen content
WT
DKO
I
Day 9
Relative collagen content
WT
DKO

**Figure S3. Normal TF, (myo)fibroblasts, and collagen content in DKO during the course of skin wound healing.** (A) Immunohistochemistry staining of tissue factor (brown) at day 3 post-injury. TF = tissue factor. Scale bar = 50 μm. (B) Quantification of tissue factor at day 3 post-injury (n=5-6). (C) Martius scarlet blue (MSB) staining of skin wound at day 1 post-injury. Red = old fibrin, blue = collagen, yellow = red blood cells/fresh fibrin. Scale bar = 200 μm. (D) Quantification of fibrin content in the wound at day 1 post-injury (n=5). (E) Immunofluorescence staining of (myo)fibroblasts (vimentin$^+$ cells; red) in the wound of WT and DKO mice at day 3 (n=4) and day 9 post-injury (n=3). Hoechst counterstains nuclei (blue). Scale bar = 20 μm. (F) Quantification of (myo)fibroblasts (vimentin$^+$ cells) at day 3 post-injury (n=4). (G) Quantification of (myo)fibroblasts (vimentin$^+$ cells) at day 9 post-injury (n=3). (H) Quantification of collagen content (blue color) in MSB staining within the wound at day 3 post-injury (n=7-9). (I) Quantification of collagen content within the scar at day 9 post-injury (n=9-13). Graphs are presented as mean ± SEM and analyzed by either one-way ANOVA with Bonferroni's multiple comparison test (B) or Student's t-test (D, F, G, H, and I).

**Figure S4**

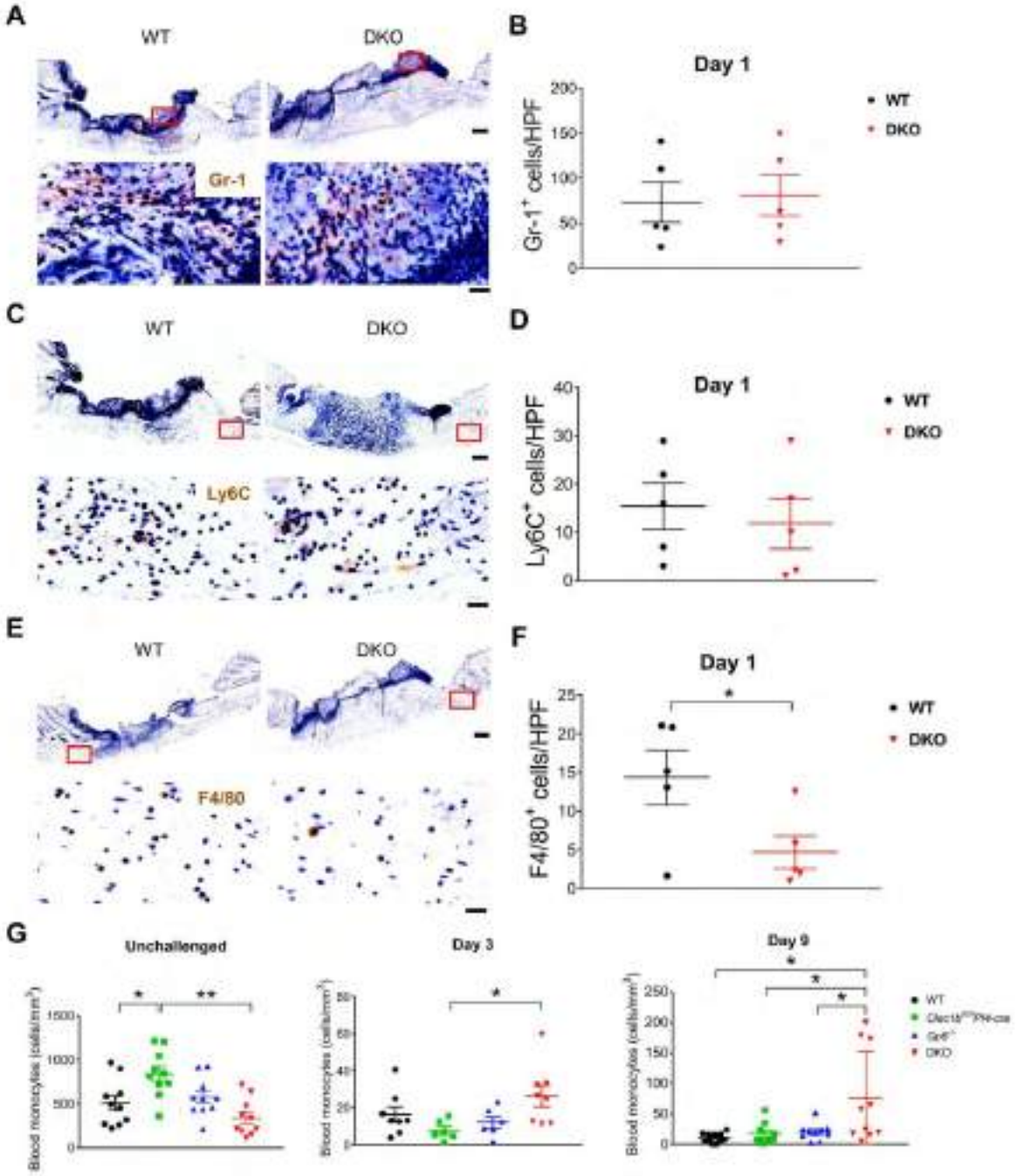
A
WT
DKO
Gr-1
B
Day 1
Gr-1+ cells/HPF
WT
DKO
C
WT
DKO
Ly6C
D
Day 1
Ly6C+ cells/HPF
WT
DKO
E
WT
DKO
F4/80
F
Day 1
F4/80+ cells/HPF
WT
DKO
G
Unchallenged
Day 3
Day 9
Blood monocytes (cells/mm3)
WT
DKO

**Figure S4. Wound neutrophils and monocytes are unaltered but macrophage influx is decreased in DKO mice at day 1 post-injury.** (A) Staining of neutrophils (Gr-1; brown) in wound area at day 1 post-injury. (B) Quantification of neutrophils (Gr-$1^+$ cells) in wound area at day 1 post-injury (n=5). (C) Staining of monocytes ($Ly6C^+$; brown) in wound area at day 1 post-injury. (D) Quantification of monocytes ($Ly6C^+$ cells) in wound area at day 1 post-injury (n=5). (E) Detection of macrophages (F4/80 staining; brown) in wound area at day 1 post-injury. (F) Quantification of macrophages ($F4/80^+$ cells) in wound area at day 1 post-injury (n=5). (G) Comparison of blood monocytes between all groups at baseline (left), day 3 (middle), and day 9 post-injury (right). Graphs are presented as mean ± SEM and analyzed by either Student's t-test (B, D, and F) or one-way ANOVA with Bonferroni's multiple comparison test (G). *$p<0.05$, **$p<0.01$*. Scale bar = 200 μm (upper panel), and 20 μm (lower panel).

**Figure S5**

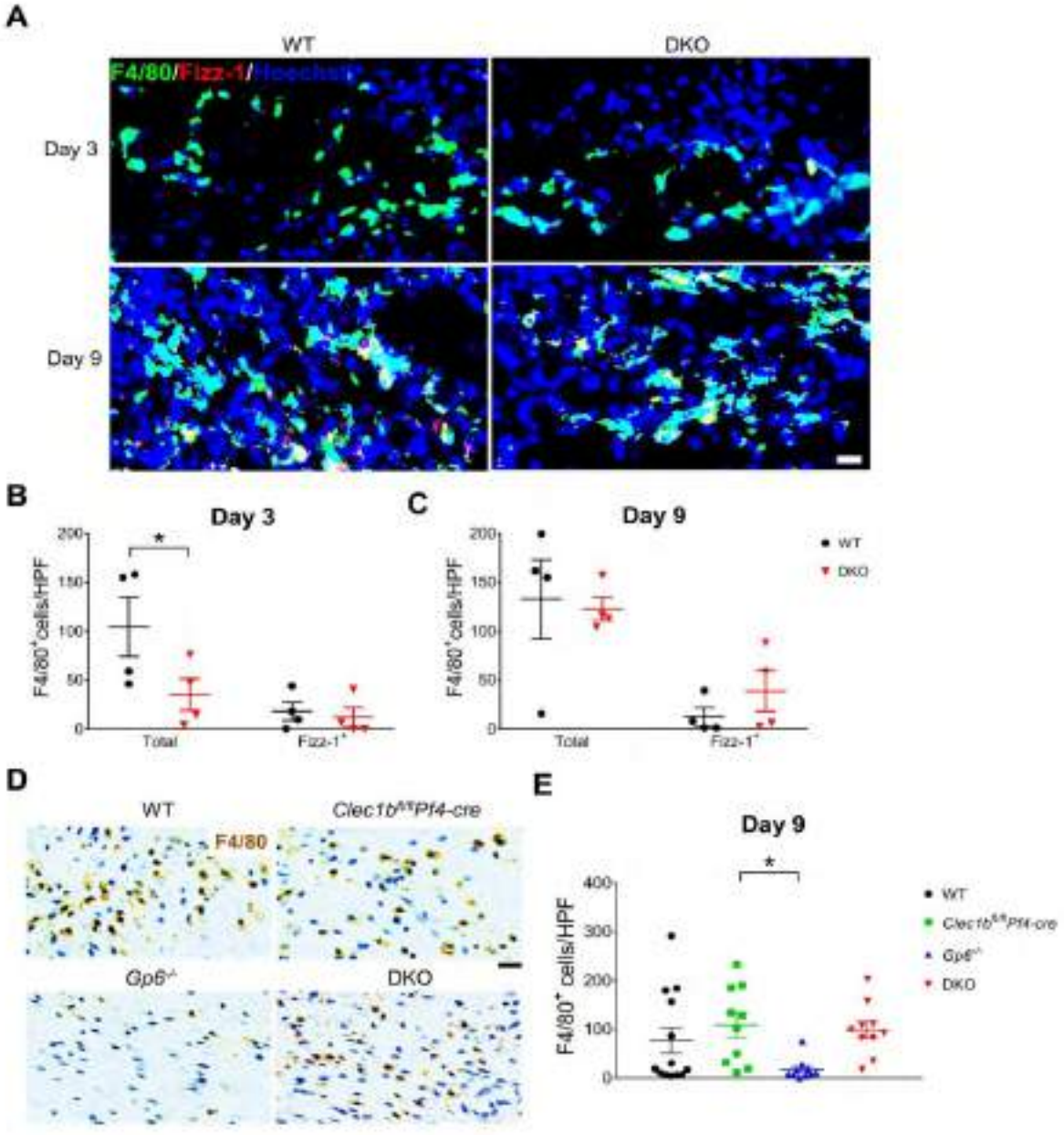
A
WT
DKO
F4/80/Fizz-1/Hoechst
Day 3
Day 9
B
Day 3
F4/80+cells/HPF
Total
Fizz-1+
C
Day 9
WT
DKO
D
WT
Clec1b fl/fl Pf4-cre
F4/80
Gp6-/-
DKO
E
Day 9
WT
Clec1b fl/fl Pf4-cre
Gp6-/-
DKO

**Figure S5. Normal M2 macrophage recruitment in DKO mice during the course of wound healing.** (A) Immunofluorescence double staining of Fizz-1 (red) and F4/80 (green) in the wound of WT and DKO mice at day 3 (n=4) and day 9 post-injury (n=4). Hoechst counterstains nuclei (blue). Scale bar = 20 µm. (B) Quantification of M2 macrophages (Fizz-$1^{+}$F4/$80^{+}$ cells; yellow) at day 3 post-injury (n=4). (C) Quantification of M2 macrophages (Fizz-$1^{+}$F4/$80^{+}$ cells; yellow) at day 9 post-injury (n=4). (D) Detection of F4/$80^{+}$ cells (brown) in wound at day 9 post-injury. Scale bar = 20 µm. (E) Quantification of F4/$80^{+}$ cells in wound at day 9 post-injury (n=10-13). Graphs are presented as mean ± SEM and analyzed by either Student's t-test (B and C) or one-way ANOVA with Bonferroni's multiple comparison test (E). *$p < 0.05$.

**Figure S6**

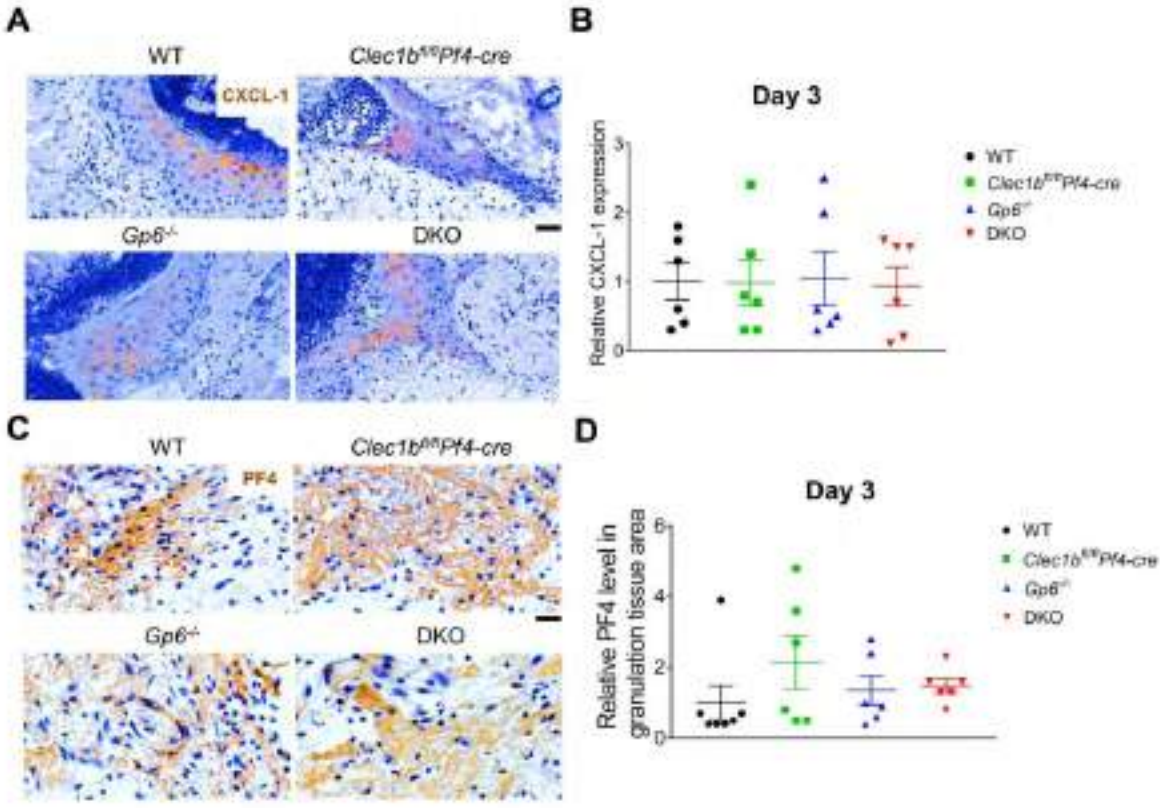


**Figure S6. Normal expression of CXCL-1 and PF-4 at day 3 post-injury in DKO mice.** (A) Detection of CXCL-1 (brown) in wound area at day 3 post-injury. (B) Quantification of keratinocyte-expressed CXCL-1 in wound area at day 3 post-injury (n=6). (C) Detection of PF4 (brown) in wound area at day 3 post-injury. (D) Quantification of PF4 within the granulation tissue in wound area at day 3 post-injury (n=6). Data are presented as mean ± SEM and analyzed by one-way ANOVA with Bonferroni's multiple comparison test. Scale bar = 20 μm.

**Figure S7**

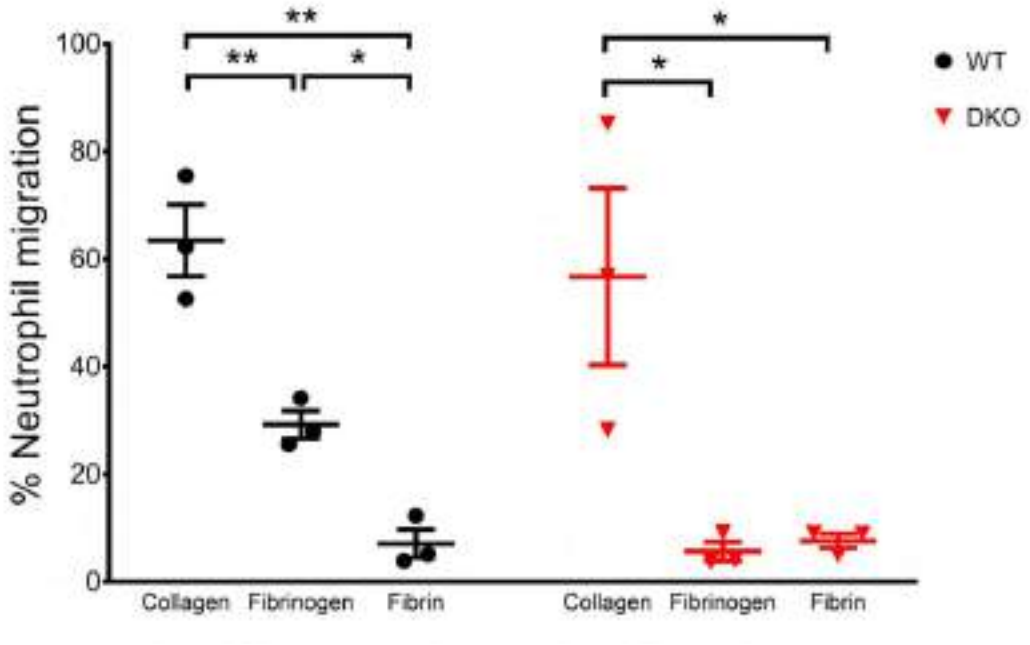


**Figure S7. Fibrinogen and crosslinked fibrin matrix attenuate neutrophil chemotaxis *in vitro*.** Graphs represent migration of neutrophils through collagen, fibrinogen, and fibrin matrix (n=3). Data are presented as mean ± SEM and analyzed by one-way ANOVA. **p<0.05, **p<0.01.*

**Figure S8**

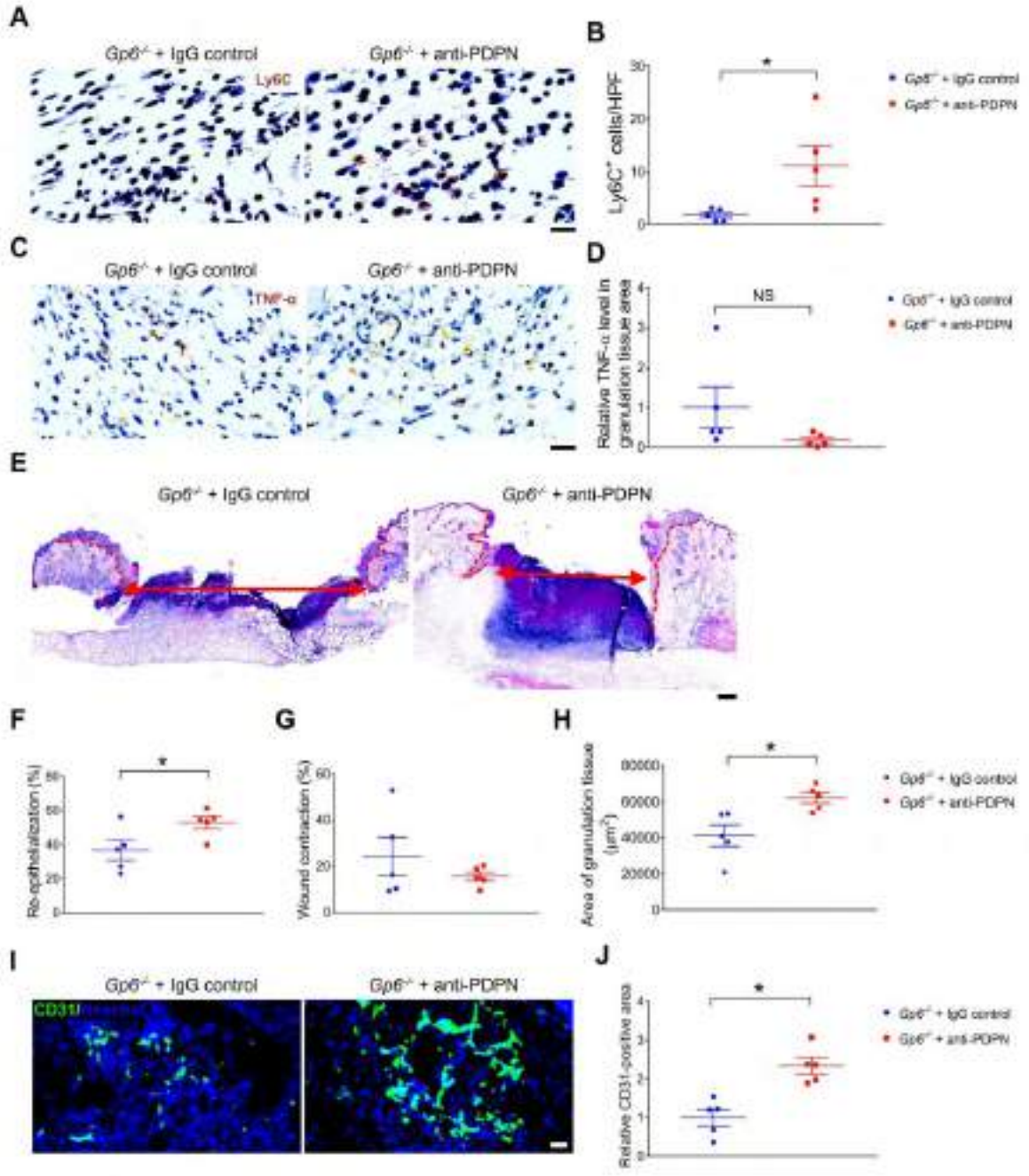
A
Gp6-/- + IgG control
Gp6-/- + anti-PDPN
Ly6C
B
Ly6C+ cells/HPF
Gp6-/- + IgG control
Gp6-/- + anti-PDPN
C
Gp6-/- + IgG control
Gp6-/- + anti-PDPN
TNF-α
D
Relative TNF-α level in granulation tissue area
NS
Gp6-/- + IgG control
Gp6-/- + anti-PDPN
E
Gp6-/- + IgG control
Gp6-/- + anti-PDPN
F
Re-epithelialization (%)
G
Wound contraction (%)
H
Area of granulation tissue (μm2)
Gp6-/- + IgG control
Gp6-/- + anti-PDPN
I
Gp6-/- + IgG control
Gp6-/- + anti-PDPN
CD31
J
Relative CD31-positive area
Gp6-/- + IgG control
Gp6-/- + anti-PDPN

**Figure S8. Increased wound monocytes, enhanced angiogenesis, rapid re-epithelialization and greater granulation tissue formation in *Gp6*$^{-/-}$ mice treated with anti-podoplanin antibody.** (A) Detection of Ly6C$^{+}$ cells (brown) in wound at day 3 post-injury. Scale bar = 20 μm. (B) Quantification of Ly6C$^{+}$ cells in wound at day 3 post-injury (n=5). (C) Immunohistochemistry staining of TNF-α (brown) in the wound at day 3 post-injury. Scale bar = 20 μm. (D) Quantification of TNF-α level in granulation tissue area at day 3 post-injury (n=5). (E) H&E staining at day 3 post-injury. Dotted line indicates hyperplastic coverages. Arrow indicates gap between epithelial tongues. Scale bar = 500 μm. (F) Measurement of re-epithelialization (n=5). (G) Measurement of wound contraction (n=5). (H) Quantification of granulation tissue area (n=5). (I) Immunofluorescence staining of endothelial cells (CD31$^{+}$ cells; green) in wound area at day 3 post-injury. Hoechst counterstains nuclei (blue). Scale bar = 50 μm. (J) Quantification of CD31$^{+}$ area within the wound at day 3 post-injury (n=5). All graphs are presented as mean ± SEM and analyzed by Student's t-test. *$p<0.05$. NS = non-significant.

**Figure S9**

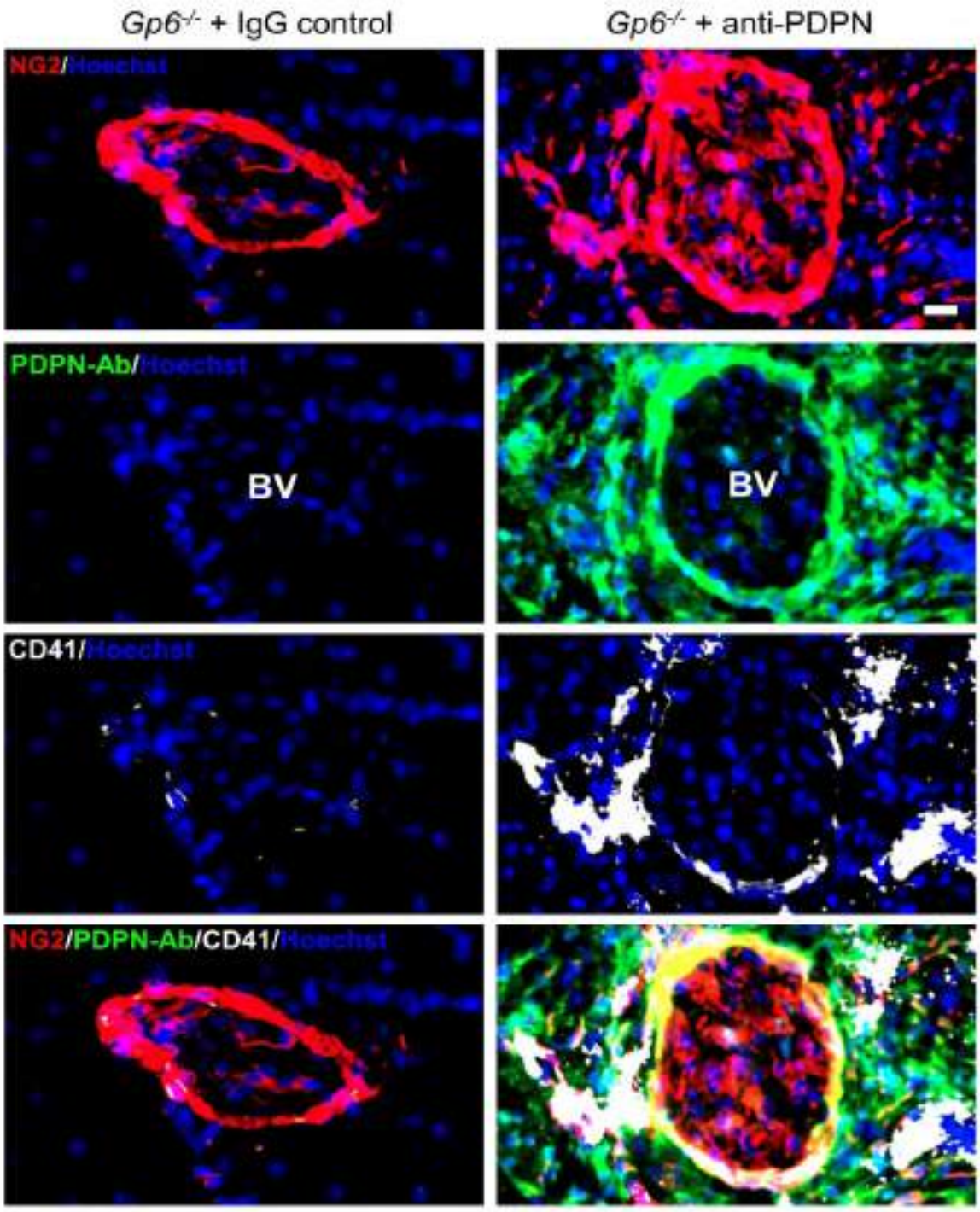
Gp6-/- + IgG control
Gp6-/- + anti-PDPN
NG2/Hoechst
PDPN-Ab/Hoechst
BV
BV
CD41/Hoechst
NG2/PDPN-Ab/CD41/Hoechst

**Figure S9. Anti-podoplanin antibody (PDPN-Ab) is detected together with extravascular platelets at perivascular area in *Gp6*$^{-/-}$ mice treated with this antibody.** Immunofluorescence staining of NG2 (red), PDPN-Ab (green) and CD41 (white) illustrates extravasation of platelets and the presence of PDPN-Ab on pericytes (NG2$^{+}$) and other cells around blood vessel at day 3 after injury (n=4-5). Alexa 488-conjugated goat anti-hamster IgG secondary antibody was used in immunofluorescence to detect the injected PDPN-Ab (clone 8.1.1.). Hoechst counterstains nuclei (blue). BV = blood vessel. Scale bar = 20 µm.

**Figure S10**

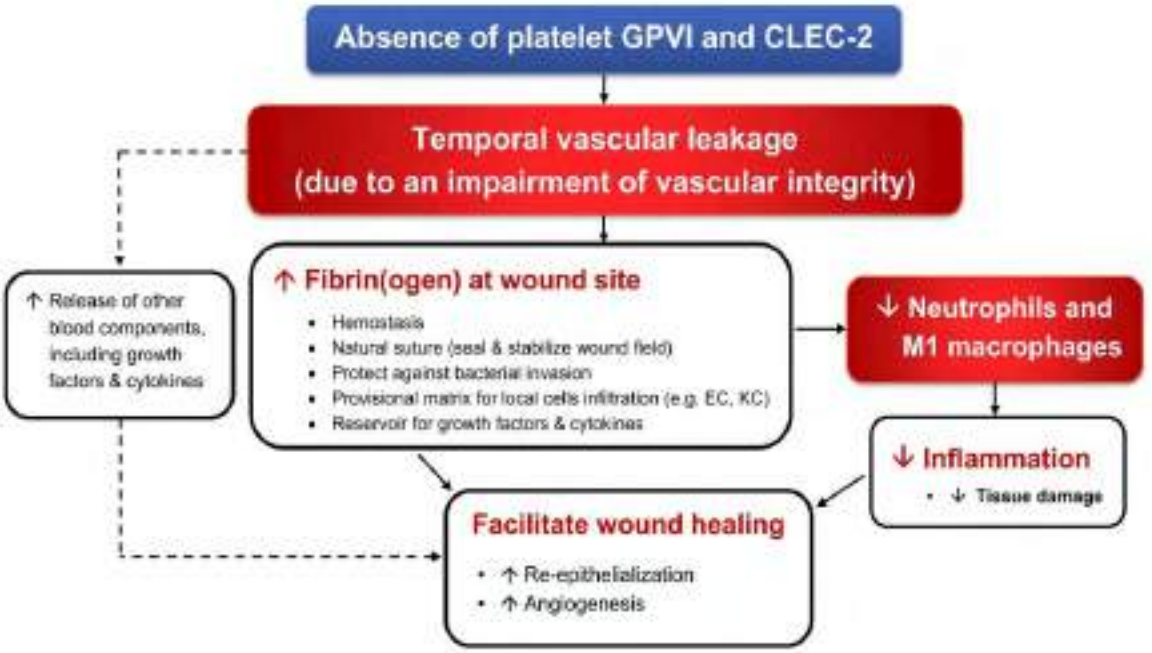


**Figure S10. Schematic illustration for multifactorial contribution of accelerated skin wound healing in the absence of platelet ITAM receptors.** A lack of GPVI and CLEC-2 results in transient vascular leakage, which contributes to higher fibrin(ogen) content at wound site. In addition, plasma-derived macromolecules (e.g. clotting factors, growth factors, and cytokines) may also leak into the wound. Moreover, ITAM-receptor deficiency decreases wound leukocytes during inflammatory phase, likely because of a physical blockade by fibrin(ogen) and a decrease in neutrophil capacity to migrate through fibrinogen, which subsequently attenuates inflammation and tissue damage. These two mechanisms associate with an accelerated skin wound healing, at least by facilitating re-epithelialization and angiogenesis. EC = endothelial cells, KC = keratinocytes.